Ocean Wave Propagation in Shallow Waters

Gabriel T Scarlett
S1040865

A thesis submitted for the degree of
Master of Mechanical Engineering
with Renewable Energy

April, 2015

Acknowledgments

I would like to acknowledge my supervisor, Professor Alistair Borthwick, who mentored and inspired me throughout my project. I received excellent direction and encouragement from him during our regular meetings, which I found to be both stimulating and enjoyable.

Most importantly, I would like to thank my wife Keiko who stood by me throughout my degree. Without her dedication and selflessness none of this would have been possible.

Personal Statement

Over the past year I have created from scratch a numerical model to solve Sobey's new set of phase-resolving integral wave evolution equations. I used Fortran to write the program and Matlab as a plotting tool.

An appreciation of fluid dynamics provided the foundation I needed to research ocean wave evolution. I identified the need to advance my mathematical knowledge to fully appreciate Sobey's equations. I worked through a derivation of The Shallow Water Equations and read literature about Boussinesq-type equations, which helped me to understand the theory. I developed my knowledge of Fortran, having previously written programmes in Matlab, Abuqus and Arduino. Professor Borthwick helped me to begin discretising terms, and gave me direction to overcome problems such as; integrating the shape factors into the model; separation of mixed derivative terms, and cnoidal wave theory. Once the model was working I had some difficulty getting the programme to run, but after decomposition of the code I identified bugs which resolved the issue.

I did not complete all of the set objectives in the given time. However, in hindsight these were quite ambitious due to the complexity of the equations being solved. This is the first time, to my knowledge, that these equations have been solved using a differencing scheme, or that harmonic analysis of two symmetrical hump disturbances has been investigated using superposition.

I am satisfied with the outcome of my work. The numerical model I present in this thesis works well for weakly non-linear waves, and can simulate both hydrostatic and dispersive wave behaviour. The foundation has been set for a model of future engineering application.

The project has taught me the importance of splitting a complex problem into smaller, less complex constituents. I have enjoyed the project very much. It has been interesting, has given me satisfaction, confidence and a good foundation to access a career in numerical modelling.

1st April 2015

Abstract

Ocean waves range from ripples on the surface to tides stretching across the ocean. In deeper water waves are dispersive which are described mathematically by Boussinesq-type equations, but in shallow water they become hydrostatic, and are given mathematically by The Shallow Water Equations. Sobey (2014), derived a new set of integral wave evolution equations, which describe both hydrostatic and dispersive waves with greater accuracy. The equations are solved numerically using the method of characteristics. This thesis outlines a new numerical model to solve them using a central differencing scheme. Difficulty in the scheme was encountered due to a mixed temporal and spatial derivative term, which is separated by matrix inversion. The model was tested for sloshing waves, which highlighted instability caused by the dispersive terms. With these switched off agreement with theory is good. The dispersion of an initial mound was used to investigate the odd and even harmonics by releasing two symmetrical humps and using superposition. This validated that the model is in agreement for linear and weakly non-linear waves. Highly non-linear terms were found to cause instability in the model. This was especially apparent when modelling in deeper water and with extreme gradients. An attempt to model progressive waves with initial conditions provided by cnoidal wave theory was unsuccessful. The numerical model works well for both non-linear and weakly-nonlinear waves. The system is limited by a central differencing scheme. It is recommended that any future work proceeds by first implementing a higher-order differencing scheme, and treating the mixed derivative term with an upwinding scheme.

Contents

Nomenclature

Roman symbols	Description	Units
A	Amplitude	[m]
B	Half width	[m]
C	Celerity	[m/s]
C	Courant number	[-]
d	Depth	[d]
D	Dispersive term	[-]
f	Coriolis acceleration	[rad m/s^2]
G	Gravitational acceleration	[m/s^2]
H	Wave height	[m]
h	Undisturbed water depth	[m]
hs	Still water depth	[m]
$\mathfrak{H}$	Depth function of h_s	[m]
i	Spatial grid point	[-]
I_n	Shape factor (n = a, p10, p11, 2)	[-]
$\mathfrak{I}$	Horizontal velocity component	[m/s]
J_1	Temporal inertia	[-]
J_2	Advective inertia	[-]
k	Temporal grid point	[-]
k	Wave number	[rad/m]
k^n	Time integration step (n= 1- 4)	[-]
L	Domain length	[m]
L	Wave length	[m]
P	Pressure	[Pa]
P_{atm}	Atmospheric pressure	[Pa]
q	Local flux	[m^2/s]
t	Time	[s]
T	Period	[s]
u	Velocity in x	[m/s]
u_{max}	Maximum velocity	[m/s]
U_R	Ursell parameter	[-]
U	Depth averaged velocity in x	[m/s]
v	Velocity in y	[m/s]
V	Depth averaged velocity in y	[m/s]
W	Velocity in z	[m/s]
x	Horizontal coordinate	[m]
X	Body force in x	[N]
y	Horizontal coordinate	[m]
y_t	Bed to trough elevation	[m]
y_s	Bed to free surface elevation	[m]
Y	Body force in x	[N]
z	Vertical coordinate	[m]

Greek symbols

α	Tensor subscript (1,2)	[-]
β	Tensor subscript (1,2)	[-]
β	Momentum correction factor	[-]
γ	Tensor subscript (1,2)	[-]
Δt	Finite change in time	[s]
Δx	Finite change in space	[m]
ε	Kinematic eddy viscosity	[Pa s]
ζ	Free surface elevation	[m]
θ	Elliptic phase	[rad]
ϑ	Elliptic amplitude	[rad]
κ	Elliptic modulus	[-]
μ	Dynamic viscosity	[Pa s]
ν	Kinematic viscosity	[m^2/s]
π	Mathematical constant	[-]
ρ	Density	[kg/m3]
Σ_w	Surface shear stress	[Pa]
Σ_b	Bed shear stress	[Pa]
τ	Shear stress	[Pa]
τ_b	Bottom shear stress	[Pa]
τ_w	Wind shear stress	[Pa]
φ	latitude	[rad]
ω	Angular velocity	[rad/s]

Uncommon functions

cn()	Jacobian cosine function
sn()	Jacobian sine function
dn()	Jacobian delta function
K()	Complete elliptic integral (1^{st})
E()	Complete elliptic integral (2^{nd})

Abbreviations

CFD	Computational fluid dynamics
CPU	Central processing unit
FD	Finite difference
FV	Finite volume
HD	Height depth
ISSC	International Ship Structures Congress
ITTC	International Tank Towing Conference
JONSWOP	Joint North Sea Wave Project
LES	Large eddy simulation
MOC	Method of characteristics
ODE	Ordinary differential equation
PDE	Partial differential equation
RANS	Reynolds-averaged Navier-Stokes
SWE	Shallow water equations
SWL	Still water level

1 Introduction and Literature Review

This chapter introduces ocean waves and describes how they propagate through shallow waters and interact with the coast. A review of literature is provided giving an overview of preceding work and the mathematical theories and numerical methods required to model ocean wave evolution. The chapter concludes by outlining the aims and objectives and a synopsis of the report thereafter.

1.1 Introduction

Ocean waves may be classified by wave period, frequency, relative amplitude, and driving force, as illustrated in Figure 1.1.

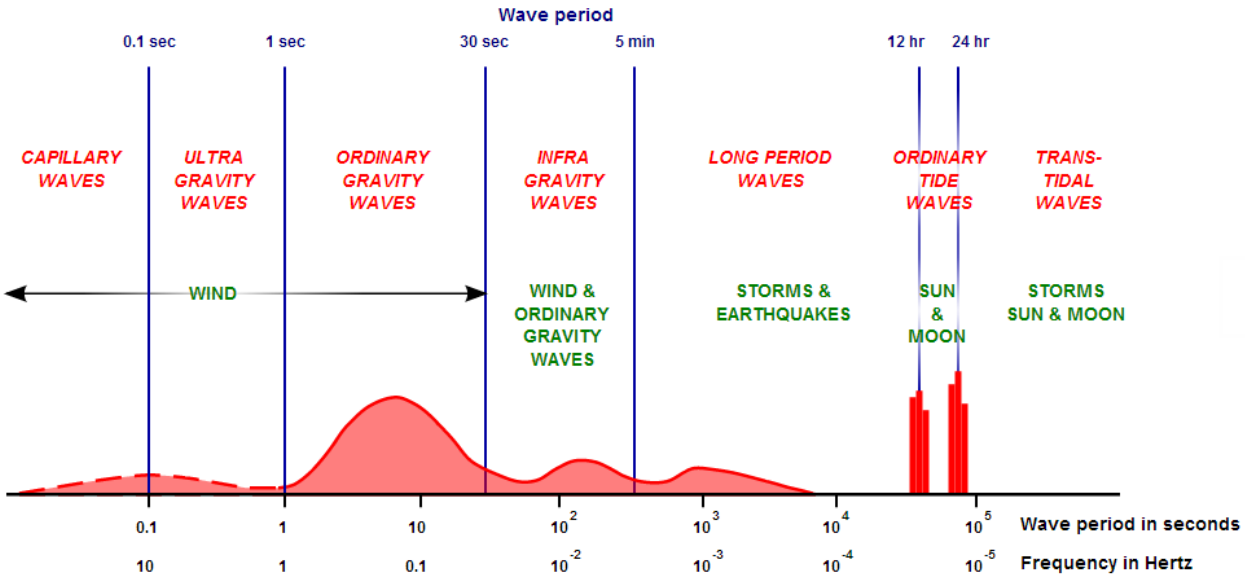

Figure 1.1. Classification of ocean waves by period, frequency, relative amplitude and driving force (Munk, 1951)

As wind flows over a smooth surface it creates capillary waves (small ripples restored under surface tension), which give the wind greater purchase, further increasing the transfer of energy. The disturbances then propagate under the restoring force of gravity. The motion becomes more unsettled as larger waves interact with turbulent air, causing fluctuating stresses and pressure gradients (Boyle, 2004). The waves become chaotic and irregular. When in phase, the oscillations combine and once large enough the wind catches the upper face of the wave like a sail, further increasing growth. Maximum wave height depends on three

factors; wind speed, duration and fetch (the range over which the wind blows). The transfer of energy ceases once a wave is travelling at a celerity equal or greater than the wind speed. These waves, known as swell, leave the fetch as a series of wave trains. Pressure systems can also develop long waves, where in regions of large atmospheric temperature gradients, areas of low pressure occur, causing the ocean to bulge. Combined with high tides and winds, this can result in storm surges where a rise in local water depth at the coast brings large unbroken waves closer to the shore with devastating effect. One of the worst such events was in 2013 when Typhoon Haiyan flooded the islands of Leyte, Bohol, and Cebu in the Philippines. Tides are caused by the motion of the earth, moon and sun, which results in a gravitational force imbalance causing the sea to bulge up on either side of the earth. Tides are made up of two dominant cycles; semi-diurnal and spring-neap, both of which can be predicted with great accuracy. The resulting long waves stretch across the ocean travelling at vast speeds, but at the coast they are normally treated as a temporal difference in water elevation. Tsunami are caused by landslides, or seismic events, which displace large volumes of water in the ocean. In deep water tsunamis are long waves with small crests and barely noticeable troughs. However when tsunamis reach the coast they rise up as solitary waves with great crests and small troughs before breaking up into turbulent bores (Borthwick et al., 2006a). The tsunami of 2011 produced by an earthquake off the Japanese Pacific coast caused mass devastation and loss of life throughout the prefecture of Tohoko.

Waves transport energy, rather than the medium in which they propagate. Water particles in a wave travel in orbits which decrease in size with depth. Ocean waves are not pure waves since the positive flow of the crest is greater than the negative flow of the trough which results in a net transport of the medium. A current, known as the Stokes drift results. Longuet-Higgins and Stewart (1964), explain wave-current phenomena at the shore in terms of radiation stress which describe excess momentum flux (due to the orbital motion of individual water molecules, which cause a force in the direction of propagation, and at right angles to it). Radiation fluxes are responsible for set-up and set-down; local slopes in the water level due to the presence of waves, which can in turn cause infragravity waves; and long waves reflected back out to sea. The theory also explains longshore currents which run parallel to the shoreline (Reeve et al., 2004). These mechanisms are often responsible for rip currents, where at certain points along the shore opposing longshore currents meet and the resulting jet flows back out to sea. Other wave-induced currents include boundary layer drift, and undertow. Waves also interact with ocean currents and tides, which alter them physically and directionally.

Waves can be further classified by the depth of water in which they propagate, in relation to their wavelength as shown in Table 1.1.

Table 1.1. Classification of ocean waves by ratio of water depth to wavelength for deep, transitional and shallow water waves.

Classification	h_s/L
Deep water	$> 1/2$
Transitional	$1/20\ to\ 1/2$
Shallow	$< 1/20$

Most waves which propagate through shallow waters can be described as long waves in which wavelength is much greater than water depth. Most ocean waves are progressive. Swell waves can propagate for many hundreds of kilometres whilst retaining most of their energy. In deep water, wave trains travel in groups with long waves at the helm and shorter ones at the rear. This dispersion occurs because in deep water the celerity of a wave is proportional to its wavelength. As the water shallows, wave particle orbits begin to feel the bottom and dissipate energy through friction, at which point the celerity becomes a function of both water depth and wavelength. Once in shallow water, waves become hydrostatic where celerity is related to depth only. The waves decrease in speed and wavelength and increase in height, they are reflected and refracted towards or away from shore, and diffracted by peninsulas, islands and breakwaters. Waves shoal and their height reaches a limit and breaks. The remaining energy is dissipated through run-up at the shoreline. Standing waves known as seiches may also occur when waves propagating in enclosed areas such as harbours and ocean basins are reflected back in the direction of propagation, causing standing waves which oscillate up and down. These seiches are normally of very long wavelength and small amplitude, so often go unnoticed. However they can amplify when in phase with the natural frequency of channels and harbours, giving rise to resonance. Waves can also be forced to propagate out in all directions from a single source. This occurs when a large pressure system or seismic event disturbs a body of water, creating a mound which then falls in on itself causing waves to disperse outwards from the centre.

Waves and tides govern coastal morphology; through the constant transportation of sediment, beaches are created and depleted, cliff faces are eroded and civil facilities affected by sediment build up. This can take place over very short periods during storms, seasonally, or over much longer time scales when man-made influences on the coast also become apparent. There are two main modes of transportation. Bed shear which causes the sediment to move along the floor, and which in turn is responsible for the ripples found in wet sand on the beach at low tide. The other mode is the suspension of particles in moving water which are transported by mechanisms such as Stokes drift, longshore currents, and undertow. With 65%

of mega cities located in coastal zones, damage to civil infrastructure from the sea can have a global economic impact. Sea defences are required to protect residential areas, industry, transportation networks, and places of recreation from flooding. The biggest present threat facing coastal regions and low-lying island nations is the rise in sea levels as a result of melting ice caps brought on by climate change (Thorne et al., 2007). This will increase tidal range and bring more wave breakers to shore. With 10% of the world's population living just 10 m above sea level, a small rise can present a massive threat (Oliver-Smith, 2009).

Presently the drive for clean renewable energy has brought about research and development of technologies that can harness energy from the marine environment. Near the coast, tidal barrages and tidal current devices can harness the potential and kinetic energy of the tides, and oscillating water columns or flaps can harness the power of shore-bound waves.

Technological advances in computing power enable engineers to model numerically how the sea interacts with civil infrastructure. In order to better protect the coastal environment from future climate change and to estimate accurately the energy resource available from the marine environment, enhanced numerical models applicable over a greater range, are required to increase the accuracy of simulations.

1.2 Review of Literature on Wave Evolution

To capture the full three-dimensional structure of a water column would require modelling the full Navier-Stokes equations with a turbulence model such as Reynolds-averaging (RANS) or Large Eddy Simulation (LES). An investigation into the 3D flow structure of a turbine plane modelling a single turbine in a channel of 1.5 m width, 0.8 m depth and 24 m in length required 281 and 1340 CPU hours for RANS and LES respectively (Tully and Ingram, 2014). Thus the engineering benefits of estimating the vertical flow structure is great.

A plethora of wave theories exist. One of the most widely-used is linear wave theory derived by Airy in 1841. The basis of this theory are the Laplace and the Euler-Bernoulli momentum equations, assuming an inviscid fluid and potential flow. Nonlinear terms are dropped from the derivation by assuming slow particle velocities (Mehaute, 1976). The resulting equations give good approximations of wave motion for small relative wave heights over a horizontal bed.

Ursell (1953) determined a parameter whereby the non-linearity of a wave could be established, and showed that for linear theory to be valid the following must hold:

$$U_R = \frac{HL^2}{d^3} \ll 1\,. \tag{1.1}$$

As shown in Figure 1.2 the Ursell parameter is always greater than unity in intermediate water depth, and of a much greater order in shallow waters. Therefore, unless both the relative wave height and depth are small, non-linear terms cannot be ignored in shallow water.

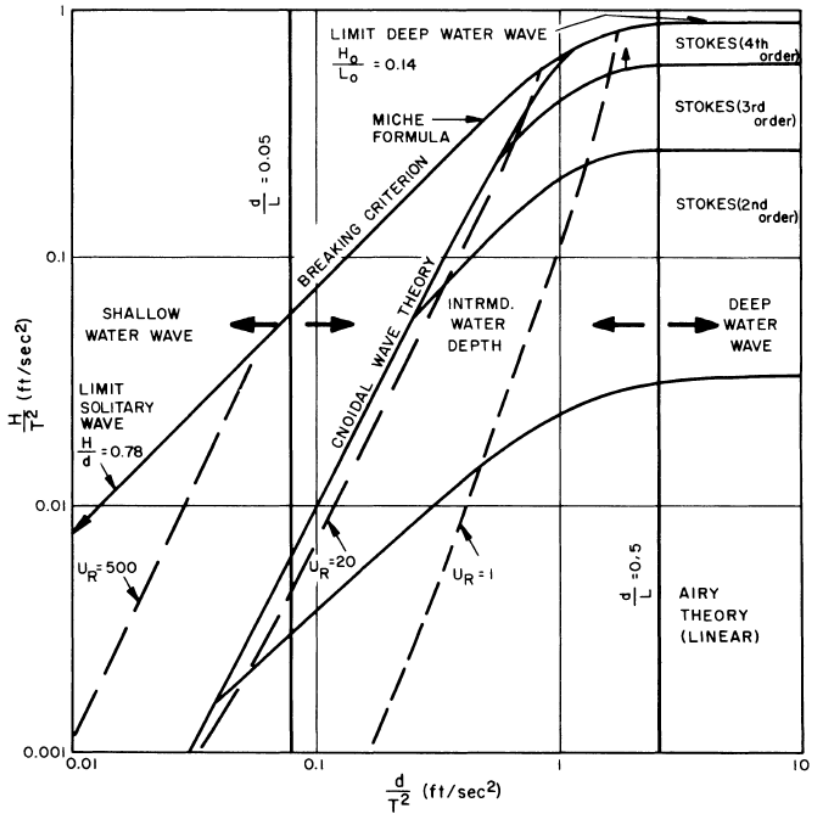

Figure 1.2. Limits of wave theories for wave height, depth and wavelength, showing Ursell parameter (Mehaute, 1976)

Adaptations to linear theory, such as the mild slope equation, derived by Berkoff (1972) which approximates the vertical motion of a linear wave over a gentle bathymetry, enable non-linear behaviour such as diffraction, refraction, scattering, and shoaling to be modelled. Further modifications such as that of Chamberlain and Porter (1995) include the addition of correction coefficients and weakly non-linear terms to better predict wave scattering.

Cnoidal wave theory is used to describe progressive wave evolution for $U_R > 20$ as shown in Figure 1.2. First described by Korteweg and de Vries (1895) and termed cnoidal due to the surface elevation being proportional to the square of the Jacobian elliptic cosine function, cn.

Original first order theories are given by Keulegan and Patterson (1940). The theory was later advanced for practical application by Wiegel (1960) who presented full mathematical approximations. The complexity of the elliptic functions has restricted the use of cnoidal theory. Iwagaki (1968) addressed the problem by transforming the elliptic functions into hyperbolic functions. Further higher order theories are given by Fenton (1979) and more recently Sobey (2012).

Two integral wave evolution theories exist which describe non-linear wave evolution in shallow water; The Shallow Water Equations (SWE) which describe hydrostatic waves, and Boussinesq-type equations which describe dispersive waves. Both assume shallow water (see Table 1.1), whereby the horizontal velocity component of the flow is deemed to be of a greater order than the vertical structure, allowing the flow to be transformed into two height dimensions (2HD), by depth-averaging.

The Reynolds-averaged Navier-Stokes equations, obtained by spatially averaging turbulent fluctuations in the flow field, are the basis of the SWE given by Falconer (1993). Modelling turbulence is important for fast flowing channel flows, wave breaking and overtopping. However for large coastal basins, it is often assumed that the flow is dominated by large body or frictional forces, such that the flow can be assumed to be inviscid and depth-averaging of the Euler equations is appropriate (Dean and Dalrymple, 1991). An alternative derivation is given by Abbott (1979) who uses mass conservation and an elemental momentum balance to derive the classical 1HD inviscid Saint Venant equation.

Boussinesq (1872) derived a version of shallow water equations in response to the nonlinear wave behaviour first described by John Scott Russell in 1834, who observed a large mass of water being set in motion and travelling as a solitary wave on an Edinburgh Canal. The basis of the derivation is the depth-averaging of the Laplace or Euler equations, then using a polynomial expansion to estimate the vertical dispersive structure in terms of the ratio of depth to wavelength and amplitude, the accuracy depends on the order of terms. An early version by Peregrine (1967) gives an accurate representation of weakly non-linear and weakly dispersive waves. Modern equations striving for improved dispersion and range of water depth become increasingly complex. A higher-order set with improved linear dispersion properties are the equations derived by Madsen and Sørensen (1992). The version derived by Wei et al. (1995) gives momentum in 10 terms, and a further extension by Madsen and Schäffer (1998) gives 7 terms in mass conservation and 18 in momentum conservation. Thus the equations have become ever more complex for a 2HD model not designed for deep water.

Hybrid models linking SWE and Boussinesq exist. That of Borthwick et al. (2006a) captures the run-up and breaking action of solitary waves by linking up both SWE and Boussinesq equations. Similarly the hybrid model of Orszaghova et al. (2011) couples solitary and dispersive waves with wave breaking action. Both hybrid models are solved with a Godunov-type finite volume method.

The phase-resolving integral equations of Sobey (2014) are a single set of equations describing both hydrostatic and dispersive behaviour over a broad range of depths. The basis is depth-averaging of the mass and momentum equations, but the pressure term is examined by expanding the vertical momentum equation to introduce further dispersive terms. These terms are then dealt with by heuristic scaling and matching phase against theory for progressive waves, and assigning shape factor coefficients. The equations are then solved using the method of characteristics (MOC) which transform a set of partial differential equations (PDE) into a set of ordinary differential equations (ODE) passing along a characteristic line. This method gives enhanced stability as it does not force linearization.

1.3 Aim and Objectives

The overall aim of the project is to create a numerical model using finite differences to solve Sobey's phase-resolving integral wave evolution equations. If successful, this model will provide solutions to both short and long gravity waves, with a considerable increase in accuracy compared to the non-linear shallow water or Boussinesq-type models. The greater benefits are that tidal energy resource can be better predicted; the consequence of sea levels rise can be modelled more accurately to better protect island nations, coastal infrastructure and tsunami propagation can be better understood, and, possibly lead to faster models and better early warning systems.

The objectives to achieve the task are:

- Development of a finite difference solver for the shallow water equations.
- Development of a finite difference solver for Sobey's equations.

The model will then be verified by applying it to the following examples of wave evolution:

- Sloshing waves in a tank
- Steady progressive wave evolution
- Dispersion of an initial mound

A parameter study will be carried out to investigate the sensitivity of the numerical model.

1.4 Synopsis

The remainder of the thesis is laid out as follows. Chapter 2 provides a comprehensive derivation of the shallow water equations, introduces two Boussinsq-type models from the literature, and gives a description of the mathematical model derived by Sobey (2014) that forms the cornerstone of the project. Chapter 3 outlines the numerical model required to solve Sobey's equations by discretising spatial and temporal derivatives. Chapter 4 describes the methodology and results for three wave evolution tests: wave sloshing, progressive waves and dispersion of an initial mound (the Cauchy-Poisson problem). The chapter concludes with a short interpretation of the results. Chapter 5 provides a summary of the key findings and concludes with future recommendations.

2 Mathematical Description

In this chapter, derivations are provided for SWE, Sobey's phase-resolving integral wave evolution equations, and Cnoidal wave theory. Two Boussinesq-type equations of varying complexity are also introduced.

2.1 Boundary Conditions

Consider the water column shown in Figure 2.1, where ζ is the free surface elevation, h_s is the still water level depth, and the total depth $h = h_s + \zeta$. The z-coordinate is measured upwards from the still water level (SWL).

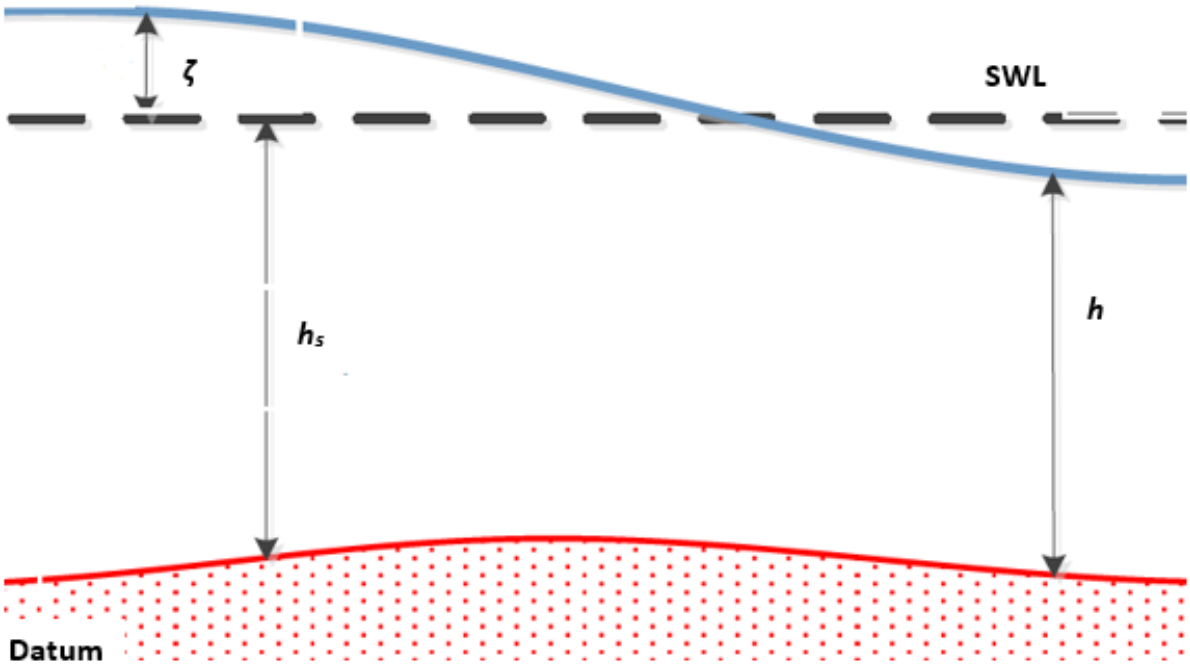

Figure 2.1. Schematic of water column

The dynamic condition at the free surface is that the pressure is atmospheric. The kinematic condition stipulates that a particle remains at the free surface, such that the vertical velocity is given by the rate of change of the free surface:

$$w(x,y,\zeta) = \frac{\partial \zeta}{\partial t} + u(x,y,\zeta)\frac{\partial \zeta}{\partial x} + v(x,y,\zeta)\frac{\partial \zeta}{\partial y} \ . \tag{2.1}$$

For a fixed bed, there is no flow at the bottom such that:

$$w(x,y,-h_s) = -u(x,y,-h_s)\frac{\partial h_s}{\partial x} - (x,y,-h_s)\frac{\partial h_s}{\partial y} \ . \tag{2.2}$$

2.2 Shallow Water Equations

It is assumed that the fluid is incompressible and that the pressure distribution is hydrostatic.

The Reynolds-averaged continuity equation is given by Equation 2.3:

$$\frac{\partial \bar{u}}{\partial x} + \frac{\partial \bar{v}}{\partial y} + \frac{\partial \bar{w}}{\partial z} = 0 \ , \tag{2.3}$$

where the overbar denotes a time-averaged quantity. Integrating Equation 2.3 from the still water depth to the free surface elevation (where the overbars have been dropped for convenience) gives:

$$\int_{-h_s}^{\zeta} \left(\frac{\partial u}{\partial x} + \frac{\partial v}{\partial y} + \frac{\partial w}{\partial z}\right) dz = \int_{-h_s}^{\zeta} \frac{\partial u}{\partial x} dz + \int_{-h_s}^{\zeta} \frac{\partial v}{\partial y} dz + w(x,y,\zeta) - w(x,y,-h_s) = 0 \ . \tag{2.4}$$

This is simplified by using Leibniz's formula for the differentiation of an integral, given as:

$$\frac{\partial}{\partial x}\int_b^a f(x,y)dy = -f(x,b)\frac{\partial b}{\partial x} + f(x,a)\frac{\partial a}{\partial x} + \int_b^a \left[\frac{\partial}{\partial x} f(x,y)\right] dy \ . \tag{2.5}$$

Applying the formula to Equation 2.4 gives:

$$\begin{aligned} &\frac{d}{dx}\int_{-h_s}^{\zeta} u \, dz - u(x,y,\zeta)\frac{\partial \zeta}{\partial x} - u(x,y,-h_s)\frac{\partial h_s}{\partial x} + w(x,y,\zeta) - w(x,y,-h_s) \\ &\qquad + \frac{d}{dy}\int_{-h_s}^{\zeta} v \, dz - v(x,y,\zeta)\frac{\partial \zeta}{\partial y} - v(x,y,-h_s)\frac{\partial h_s}{\partial v} = 0 \ . \end{aligned} \tag{2.6}$$

Defining the depth-averaged velocity components using the integral definition for a mean value give:

$$U = \frac{1}{h}\int_{-h_s}^{\zeta} u \, dz \ , \tag{2.7}$$

and

$$V = \frac{1}{h}\int_{-h_s}^{\zeta} v \, dz \ . \tag{2.8}$$

Substituting the depth-averaged velocity components along with the free surface and fixed bed boundary conditions (Equation 2.1 and Equation 2.2) into Equation 2.6 gives the depth averaged mass conservation equation:

$$\frac{\partial \zeta}{\partial t} + \frac{\partial (Uh)}{\partial x} + \frac{\partial (Vh)}{\partial y} = 0\,. \tag{2.9}$$

The *x*-component of RANS is given as:

$$\begin{aligned} \frac{\partial \bar{u}}{\partial t} + \frac{\partial \overline{u^2}}{\partial x} + \frac{\partial \overline{uv}}{\partial y} + \frac{\partial \overline{uw}}{\partial z} &= \bar{X} - \frac{1}{\rho}\frac{\partial \bar{p}}{\partial x} \\ + \frac{1}{\rho}\left[\frac{\partial}{\partial x}\left(\mu\frac{\partial \bar{u}}{\partial x} - \rho\overline{u'u'}\right) + \frac{\partial}{\partial y}\left(\mu\frac{\partial \bar{u}}{\partial x} - \rho\overline{u'v'}\right) + \frac{\partial}{\partial z}\left(\mu\frac{\partial \bar{u}}{\partial x} - \rho\overline{u'w'}\right)\right]\,. \end{aligned} \tag{2.10}$$

The fluctuating terms denoted by a prime are the Reynolds apparent stresses. These terms can be simplified by applying the Boussinesq hypothesis, relating kinematic eddy viscosity to apparent stresses where:

$$-\rho\overline{u'u'} = \varepsilon\rho\left(\frac{\partial \bar{u}}{\partial y} + \frac{\partial \bar{u}}{\partial x}\right), \tag{2.11}$$

$$-\rho\overline{u'v'} = \varepsilon\rho\left(\frac{\partial \bar{u}}{\partial y} + \frac{\partial \bar{v}}{\partial x}\right), \tag{2.12}$$

and

$$-\rho\overline{u'w'} = \varepsilon\rho\left(\frac{\partial \bar{u}}{\partial y} + \frac{\partial \bar{w}}{\partial x}\right). \tag{2.13}$$

Applying the approximation and manipulating Equation 2.10 becomes:

$$\begin{aligned} \frac{\partial \bar{u}}{\partial t} + \frac{\partial \overline{u^2}}{\partial x} + \frac{\partial \overline{uv}}{\partial y} + \frac{\partial \overline{uw}}{\partial z} &= \bar{X} - \frac{1}{\rho}\frac{\partial \bar{p}}{\partial x} \\ + \left[\frac{\partial}{\partial x}(\varepsilon + \upsilon)\left[2\frac{\partial \bar{u}}{\partial x}\right] + \frac{\partial}{\partial y}(\varepsilon + \upsilon)\left[\frac{\partial \bar{u}}{\partial y} + \frac{\partial \bar{v}}{\partial x}\right] + \frac{\partial}{\partial z}(\varepsilon + \upsilon)\left[\frac{\partial \bar{u}}{\partial z} + \frac{\partial \bar{w}}{\partial x}\right]\right]\,. \end{aligned} \tag{2.14}$$

Integrating from the still water depth to the free surface (again dropping overbars for convenience) gives:

$$\begin{aligned} \int_{-h_s}^{\zeta}\left(\frac{\partial u}{\partial t} + \frac{\partial u^2}{\partial x} + \frac{\partial uv}{\partial y} + \frac{\partial uw}{\partial z}\right)dz &= \int_{-h_s}^{\zeta}(X)\,dz - \frac{1}{\rho}\int_{-h_s}^{\zeta}\left(\frac{\partial p}{\partial x}\right)dz \\ + \int_{-h_s}^{\zeta}\left[\frac{\partial}{\partial x}(\varepsilon + \upsilon)\left[2\frac{\partial u}{\partial x}\right] + \frac{\partial}{\partial y}(\varepsilon + \upsilon)\left[\frac{\partial u}{\partial y} + \frac{\partial v}{\partial x}\right] + \frac{\partial}{\partial z}(\varepsilon + \upsilon)\left[\frac{\partial u}{\partial z} + \frac{\partial w}{\partial x}\right]\right]dz\,. \end{aligned} \tag{2.15}$$

Equation 2.15 is simplified by making the observation that $\varepsilon \gg \nu$, and approximating that:

$$\frac{\partial}{\partial x}\int_{-h_s}^{\zeta} \varepsilon \frac{\partial u}{\partial x}\, dz = \frac{\partial}{\partial x}\left[\bar{\varepsilon} h \frac{\partial U}{\partial x}\right]. \tag{2.16}$$

After applying Leibnitz's formula, the kinematic boundary conditions, and depth-averaged velocity components, the momentum equation becomes:

$$\frac{\partial (Uh)}{\partial t} + \frac{\partial (\beta_{xx} U^2 h)}{\partial x} + \frac{\partial \left(\beta_{yx} UVh\right)}{\partial y} = \int_{-h_s}^{\zeta} (X)\, dz - \frac{1}{\rho}\int_{-h_s}^{\zeta} \left(\frac{\partial p}{\partial x}\right) dz + \frac{\tau_{wx} - \tau_{bx}}{\rho} + 2\frac{\partial}{\partial x}\left[\bar{\varepsilon} h \frac{\partial U}{\partial x}\right] + \frac{\partial}{\partial y}\left[\bar{\varepsilon} h \left[\frac{\partial U}{\partial y} + \frac{\partial V}{\partial x}\right]\right], \tag{2.17}$$

where τ_{wx} and τ_{bx} are the surface wind stress and bed stress components respectively. And the β momentum factors are:

$$\beta_{xx} = \frac{1}{hU^2}\int_{-h_s}^{\zeta} u^2\, dz\,,$$

and

$$\beta_{yx} = \frac{1}{hUV}\int_{-h_s}^{\zeta} uv\, dz\,,$$

which correct for the squared depth averaged velocities.

By scaling, the *z*-momentum equation becomes:

$$\frac{\partial p}{\partial z} = \rho g\,. \tag{2.18}$$

Integrating gives the hydrostatic pressure distribution:

$$p = \rho g(\zeta - z) + p_{atm}\,. \tag{2.19}$$

Differentiating and assuming constant atmospheric pressure, the horizontal pressure gradient becomes:

$$\frac{\partial p}{\partial x} = \rho g \frac{\partial \zeta}{\partial x}. \tag{2.20}$$

Integration of the body force gives:

$$\int_{-h_s}^{\zeta} (X)\, dz = fVh\,, \tag{2.21}$$

where *f* is the Coriolis acceleration due to the earth's rotation given as:

$$f = 2v\omega sin\phi\,. \tag{2.22}$$

The momentum equation becomes:

$$\frac{\partial(Uh)}{\partial t} + \frac{\partial(\beta_{xx}U^2h)}{\partial x} + \frac{\partial\left(\beta_{yx}UVh\right)}{\partial y}$$
$$= 2v\omega sin\phi(Vh) - gh\frac{\partial\zeta}{\partial x} + \frac{\tau_{wx} - \tau_{bx}}{\rho} + 2\frac{\partial}{\partial x}\left[\bar{\varepsilon}h\frac{\partial U}{\partial x}\right] + \frac{\partial}{\partial y}\left[\bar{\varepsilon}h\left[\frac{\partial U}{\partial y} + \frac{\partial V}{\partial x}\right]\right]. \tag{2.23}$$

Equation 2.23 is the full parabolic-hyperbolic shallow water equation which accounts for turbulent fluctuations in the flow field. It can be simplified by setting the momentum correction factor to unity, (often found to be the case (Dean and Dalrymple, 1991)), and, assuming a large coastal domain where the turbulent stresses are small compared to bed stresses, wind shear and pressure gradients, the depth-averaged momentum equation reduces to:

$$\frac{\partial(Uh)}{\partial t} + \frac{\partial(U^2h)}{\partial x} + \frac{\partial(UVh)}{\partial y} = 2v\omega sin\phi(Vh) - gh\frac{\partial\zeta}{\partial x} + \frac{\tau_{wx} - \tau_{bx}}{\rho}, \tag{2.24}$$

with the *y*-component given similarly as:

$$\frac{\partial(Vh)}{\partial t} + \frac{\partial(V^2h)}{\partial y} + \frac{\partial(UVh)}{\partial x} = 2u\omega sin\phi(Uh) - gh\frac{\partial\zeta}{\partial y} + \frac{\tau_{wy} - \tau_{by}}{\rho}. \tag{2.25}$$

2.3 Boussinesq-type Equations

Boussinesq-type and the phase-resolving integral wave equations have many terms, and so horizontal tensor notation is adopted where α, β and γ take the values 1 and 2 to represent *x* and *y* respectively.

One of the earliest and simplest set of Boussinesq-type equations were derived by Peregrine (1967). The dependent variables are the free surface elevation $\zeta(x_\alpha, t)$, and the depth-averaged velocity components $U_\alpha(x_\alpha, t)$. Mass conservation is given as:

$$\frac{\partial \zeta}{\partial t} + \frac{\partial q_\alpha}{\partial x_\alpha} = 0\,, \tag{2.26}$$

where:

$$q_\alpha(x_\alpha, t) = U_\alpha h\,. \tag{2.27}$$

The mass conservation is then exactly that of SWE Equation 2.9. The momentum conservation equation is given by:

$$\frac{\partial U_\alpha}{\partial t} + U_\beta \frac{\partial U_\alpha}{\partial x_\beta} = -g\frac{\partial \zeta}{\partial x_\alpha} + \left\{\frac{1}{2}h_s \frac{\partial}{\partial x_\alpha}\left[\frac{\partial}{\partial x_\beta}\left(h_s \frac{\partial U_\beta}{\partial t}\right)\right] - \frac{1}{6}h_s^2 \frac{\partial}{\partial x_\alpha}\left[\frac{\partial}{\partial x_\beta}\left(\frac{\partial U_\beta}{\partial t}\right)\right]\right\}. \tag{2.28}$$

In contrast to Peregrine's set of equations are those of Wei et al (1995) where the dependent variables are $\zeta(x_\alpha, t)$, and the horizontal velocity components $\Im_\alpha(x_\alpha, t)$ at depth $\mathfrak{H} = -0.53h_s$. The mass and momentum equations are then given by Equation 2.29 and Equation 2.30 respectively:

$$\begin{aligned}\frac{\partial \zeta}{\partial t} &+ \left\{\frac{\partial (h\Im_\alpha)}{\partial x_\alpha} + \frac{\partial}{\partial x_\alpha}\left[\left(\frac{1}{2}\mathfrak{H}^2 h - \frac{1}{6}(h_s^3 + \zeta^3)\right)\frac{\partial}{\partial x_\alpha}\left(\frac{\partial \Im_\beta}{\partial x_\beta}\right)\right]\right. \\ &\left. + \frac{\partial}{\partial x_\alpha}\left[\left(\mathfrak{H}h + \frac{1}{2}(h_s^2 - \zeta^2)\right)\frac{\partial}{\partial x_\alpha}\left(\frac{\partial (h_s \Im_\beta)}{\partial x_\beta}\right)\right]\right\} = 0\,,\end{aligned} \tag{2.29}$$

$$\begin{aligned}\frac{\partial \Im_\alpha}{\partial t} &+ \left\{\Im_\beta \frac{\partial \Im_\alpha}{\partial x_\beta} + \frac{\partial}{\partial x_\alpha}\left[\frac{1}{2}\left(\frac{\partial (h_s \Im_\beta)}{\partial x_\beta} + \zeta \frac{\partial \Im_\beta}{\partial x_\beta}\right)^2\right]\right\} = -g\frac{\partial \zeta}{\partial x_\alpha} \\ &+ \left\{-\frac{1}{2}\mathfrak{H}^2 \frac{\partial}{\partial x_\alpha}\left[\frac{\partial}{\partial x_\beta}\left(\frac{\partial \Im_\beta}{\partial t}\right)\right] - \mathfrak{H}\frac{\partial}{\partial x_\alpha}\left[\frac{\partial}{\partial x_\beta}\left(h_s \frac{\partial \Im_\beta}{\partial t}\right)\right]\right. \\ &\left. + \frac{\partial}{\partial x_\alpha}\left[\frac{1}{2}\zeta^2 \frac{\partial}{\partial x_\beta}\left(\frac{\partial \Im_\beta}{\partial t}\right)\right] + \frac{\partial}{\partial x_\alpha}\left[\zeta \frac{\partial}{\partial x_\beta}\left(h_s \frac{\partial \Im_\beta}{\partial t}\right)\right]\right\} \\ &+ \frac{\partial}{\partial x_\alpha}\left[(\zeta - \mathfrak{H})\Im_\beta \frac{\partial}{\partial x_\beta}\left(\frac{\partial (h_s \Im_\gamma)}{\partial x_\gamma}\right) + \frac{1}{2}(\zeta^2 - \mathfrak{H}^2)\Im_\beta \frac{\partial}{\partial x_\beta}\left(\frac{\partial \Im_\gamma}{\partial x_\gamma}\right)\right]\,.\end{aligned} \tag{2.30}$$

The mass equation has 4 terms and the momentum equation has 10 which, as discussed in Section 1.2, is rather complex for a 2HD model.

2.4 Phase-resolving Integral Wave Evolution Equations

The approach taken by Sobey (2014) is the exact integration of the mass and momentum equations assuming an incompressible fluid, a non-turbulent regime, and the exclusion of body

forces. The same definition for mass conservation as SWE (see; Equation 2.9, or Equation 2.26 in tensor form) is arrived at. The focus is then on the momentum equations, for which the horizontal components in integral form are:

$$\rho\frac{\partial}{\partial t}\int_{-h_s}^{\zeta} u_\alpha\, dz + \rho\frac{\partial}{\partial x_\alpha}\int_{-h_s}^{\zeta} u_\alpha u_\beta\, dz = -\int_{-h_s}^{\zeta}\frac{\partial p}{\partial x_\alpha}dz + \frac{\partial}{\partial x_\beta}\int_{-h_s}^{\zeta}\tau_{\alpha\beta}\, dz + \sum_{w\alpha} - \sum_{b\alpha}\ . \tag{2.31}$$

Analysing the pressure term:

$$\int_{-h_s}^{\zeta}\frac{\partial p}{\partial x_\alpha}dz\,.$$

In SWE this is found to have a hydrostatic structure by scaling the *z*-momentum equation (see Equation 2.18) and assuming that gravity dominates. However to describe dispersive contributions, the *z*-momentum equation is integrated from an arbitrary depth *z* to the free surface. Vertical integration of the local *z*-momentum equation, and applying the Leibniz rule along with the free surface boundary conditions gives the pressure distribution as:

$$p(x_\alpha, z, t) = \rho g(\zeta - z) + \frac{\partial}{\partial t}\int_z^{\zeta}\rho w\, dz' - \rho w^2 + \frac{\partial}{\partial x_\alpha}\int_z^{\zeta}(\rho w u_\alpha - \tau_{z\alpha})\, dz' - \sum_{w\alpha} + \tau_{zz}\ , \tag{2.32}$$

where ***z'*** is a dummy variable.

Rearranging and grouping the viscous terms as p_τ, Equation 2.32 becomes:

$$p(x_\alpha, z, t) = \rho g(\zeta - z) + \frac{\partial}{\partial t}\int_z^{\zeta}\rho w\, dz' - \rho w^2 + \frac{\partial}{\partial x_\alpha}\int_z^{\zeta}\rho w u_\alpha\, dz' + p_\tau\ , \tag{2.33}$$

or, schematically:

$$p = p_g + p_1 + p_{2a} + p_{2b} + p_\tau\ , \tag{2.34}$$

where p_g is the gravity, p_1 the temporal, p_{2a} and p_{2b} the advective and p_τ the stress components, all of which contribute to vertical acceleration. Substituting Equation 2.33 and Equation 2.34 into Equation 2.31, the horizontal momentum equation becomes:

$$\rho\frac{\partial}{\partial t}\int_{-h_s}^{\zeta}u_\alpha\,dz+\rho\frac{\partial}{\partial x_\alpha}\int_{-h_s}^{\zeta}u_\alpha u_\beta\,dz=\ -\rho g h\frac{\partial\zeta}{\partial x_\alpha}+(D_1\ +D_{2a}\ +D_{2b}\ +D_\tau\ )$$
$$+\frac{\partial}{\partial x_\beta}\int_{-h_s}^{\zeta}\tau_{\alpha\beta}\,dz+\ \sum_{w\alpha}-\ \sum_{b\alpha}\,, \tag{2.35}$$

where *D* constitutes a dispersive term, which has components:

$$D_1=-\frac{1}{\rho}\int_{-h_s}^{\zeta}\frac{\partial p_1}{\partial x_\alpha}dz=\int_{-h_s}^{\zeta}\frac{\partial}{\partial x_\alpha}\left(\frac{\partial}{\partial t}\int_z^{\zeta}\rho w\,dz'\right)\,dz\ , \tag{2.36}$$

$$D_{2a}=-\frac{1}{\rho}\int_{-h_s}^{\zeta}\frac{\partial p_{2a}}{\partial x_\alpha}dz=\int_{-h_s}^{\zeta}2w\frac{\partial w}{\partial x_\alpha}\,dz\ , \tag{2.37}$$

$$D_{2b}=\frac{1}{\rho}\int_{-h_s}^{\zeta}\frac{\partial p_{2b}}{\partial x_\alpha}dz=-\int_{-h_s}^{\zeta}\frac{\partial}{\partial x_\alpha}\left(\frac{\partial}{\partial x_\beta}\int_z^{\zeta}u_\beta w\,dz'\right)\,dz\ , \tag{2.38}$$

and

$$D_\tau=-\frac{1}{\rho}\int_{-h_s}^{\zeta}\frac{\partial p_\tau}{\partial x_\alpha}dz\ . \tag{2.39}$$

Ignoring the viscous stresses the momentum equation can be represented schematically as:

$$J_1\ +\ J_2\ =G+D_1\ +D_2+(\ \sum_{w\alpha}-\ \sum_{b\alpha}\ )\,, \tag{2.40}$$

where: J_1 is temporal inertia, J_2 advective inertia, G gravitational, D_1 temporal dispersion, and $D_2 = D_{2a} + D_{2b}$ are the advective dispersive terms.

The phase variation of each term is next investigated by comparing the results of four steady progressive waves against Stokes theory in deep water and Cnoidal theory in shallow water, which give near exact solutions. The parameters of each wave are given in Table 2.1.

Table 2.1. Steady-progressive wave categories for phase evaluation

	Category	*h(m)*	*H(m)*	*T(s)*	$\omega^2 h_s/g$	$\omega^2 H/g$	H/H_{Limit}
I	Shallow	2	1	10	0.08	0.04	0.60
II	Transitional-shallow	10	4	10	0.40	0.16	0.52
III	Transitional-deep	25	7	10	1.01	0.28	0.45
IV	Deep	100	10	10	4.00	0.40	0.45

The investigation concludes that the J_2, D_1, and D_2 terms all require phase-resolution.

Advection J

By inspection the J_2 advective term is scaled as:

$$\frac{\partial}{\partial x_\alpha}\int_{-h_s}^{\zeta} u_\alpha u_\beta \, dz \sim \frac{\partial}{\partial x_\beta}\left(\frac{q_\alpha q_\beta}{h}\right) . \tag{2.41}$$

The scaling for this term is expected to be constant over the cycle, which agrees with SWE where the momentum correction factor is applied to this term. The shape factor I_a is then applied:

$$J_2 = I_a \frac{\partial}{\partial x_\beta}\left(\frac{q_\alpha q_\beta}{h}\right) , \tag{2.42}$$

The term is then phase-tested for the four waves, and the I_a coefficients assigned as least-square estimates to best match the analytical solution.

Dispersion D_1

To simplify, D_1 the vertical velocity term can be related to the horizontal velocity by vertical integration of the local mass conservation equation from the bed to an arbitrary depth z. Then using the Leibniz rule and applying the boundary conditions at the bed, the vertical velocity component becomes:

$$w(x_\alpha, z, t) = -\frac{\partial}{\partial x_\beta}\int_{-h_s}^{z} u_\alpha \, dz' . \tag{2.43}$$

Applying the definition given in Equation 2.43 for the vertical velocity, the temporal dispersion D_1 term is scaled as:

$$-\int_{-h_s}^{\zeta} \frac{\partial}{\partial x_\alpha}\left(\frac{\partial}{\partial t}\int_{z}^{\zeta} \rho w \, dz'\right) dz \sim \frac{\partial}{\partial x_\alpha}\left(\frac{\partial^2 q_\beta}{\partial t \partial x_\beta}\right) . \tag{2.44}$$

The scaling this time follows the method used in forming the Boussinesq-type equations, such as Equation 2.28 and Equation 2.30 in Section 2.3, which takes the form of length-squared:

$$\int_{-h_s}^{\zeta}\int_{-h_s}^{\zeta} \mathrm{d}z' dz = \frac{1}{2}(h_s + \zeta)^2 , \tag{2.45}$$

the first order of scaling being the squared term h_s^2. Hence:

$$D_1 = I_{p10}\frac{1}{2}h_s^2\frac{\partial}{\partial x_\alpha}\left(\frac{\partial^2 q_\beta}{\partial t \partial x_\beta}\right) . \tag{2.46}$$

As with the I_a term the I_{p10} term is a least-squares estimate to match the theory. Agreement in shallow water is good; however phase errors become considerable for the deep water wave, (*IV*). This leads to a second-order of approximation including the mixed term $h_s\zeta$ from Equation 2.45, such that:

$$D_1 = \left(I_{p10}\frac{1}{2}h_s^2 + I_{p11}h_s\zeta\right)\frac{\partial}{\partial x_\alpha}\left(\frac{\partial^2 q_\beta}{\partial t \partial x_\beta}\right) . \tag{2.47}$$

Again I_{p11} is a least squares fit to the analytical solution for progressive waves. This time agreement between phase variation is good.

Dispersion D_2

Similarly, scaling is applied to advective dispersion D_2. Such that:

$$\int_{-h_s}^{\zeta} 2w\frac{\partial w}{\partial x_\alpha}\,dz - \int_{-h_s}^{\zeta}\frac{\partial}{\partial x_\alpha}\left(\frac{\partial}{\partial x_\beta}\int_z^{\zeta} u_\beta w\,dz'\right)dz \sim \frac{\partial^2}{\partial x_\alpha \partial x_\beta}\left(\frac{q_\beta}{h}\frac{\partial q_\gamma}{\partial x_\gamma}\right) . \tag{2.48}$$

As with D_1 the first approximation is h_s^2, such that:

$$D_2 = I_{p2}\frac{1}{2}h_s^2\frac{\partial^2}{\partial x_\alpha \partial x_\beta}\left(\frac{q_\beta}{h}\frac{\partial q_\gamma}{\partial x_\gamma}\right) , \tag{2.49}$$

Again I_{p2} is a least-squares match with theory. Phase matching is good for waves I, II, and III, but worsens in deeper water. However, second-order approximation was found to be of little improvement.

Combining all terms, the final horizontal integral momentum equations are:

$$\begin{aligned}\rho\frac{\partial q_\alpha}{\partial t} + \rho I_a\frac{\partial}{\partial x_\beta}\left(\frac{q_\alpha q_\beta}{h}\right) = -\rho g h\frac{\partial \zeta}{\partial x_\alpha} + \rho\left(I_{p10}\frac{1}{2}h_s^2 + I_{p11}h_s\zeta\right)\frac{\partial}{\partial x_\alpha}\left(\frac{\partial^2 q_\beta}{\partial t \partial x_\beta}\right)\\ +\rho\, I_{p2}\frac{1}{2}h_s^2\frac{\partial^2}{\partial x_\alpha \partial x_\beta}\left(\frac{q_\beta}{h}\frac{\partial q_\gamma}{\partial x_\gamma}\right) + \sum_{w\alpha} - \sum_{b\alpha} .\end{aligned} \tag{2.50}$$

For [I_a, I_{p10}, I_{p11}, I_{p2}] = [1, 0, 0, 0], this reduces to SWE. The expansion to 1HD Cartesian form is given in Appendix A.

2.5 Cnoidal Wave Theory

Here the methodology to obtain wave profile and particle velocities from first-order cnoidal wave theory as given by Wiegel (1960) is briefly explained. Figure 2.2 shows the progressive cnoidal wave profile where y is the elevation above the bed, y_t is the elevation from the bed to the trough, y_s is the elevation to the free surface (previously denoted as h), x is the length along the domain and κ is the elliptic integral modulus. A cnoidal wave is characterised by steep crests and long flat troughs.

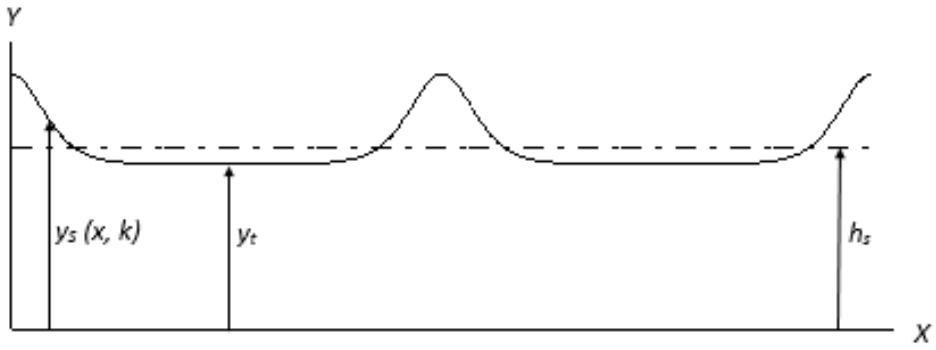

Figure 2.2. Cnoidal wave profile

The mathematical description is given in terms of the Jacobi elliptic cosine function cn(x, κ) for $0 \leq \kappa \leq 1$. This is a distorted sinusoid, where at the limits, for κ =1, the function becomes cos(x), and κ =0, becomes sech(x), resulting in a solitary wave of infinite period and wavelength. The Jacobi elliptical functions are derived from elliptical integrals of the first kind:

$$f(\kappa, \vartheta) = \int_0^{\emptyset} \frac{d\emptyset}{\sqrt{1 - k^2 sin^2 \emptyset}} \ , \tag{2.51}$$

and the second kind:

$$E(\kappa, \vartheta) = \int_0^{\emptyset} \sqrt{1 - k^2 sin^2 \emptyset} \ d\emptyset \ . \tag{2.52}$$

No analytical solutions exist for these integrals. However, numerical solutions are determined by approximating the complete elliptic integral of the first kind:

$$K(\kappa) = f\left(\kappa, \frac{\pi}{2}\right) = \int_0^{\frac{\pi}{2}} \frac{d\emptyset}{\sqrt{1 - \kappa^2 sin^2 \emptyset}} \ , \tag{2.53}$$

and second kind:

$$E(\kappa) = E\left(\kappa, \frac{\pi}{2}\right) = \int_0^{\frac{\pi}{2}} \sqrt{1 - \kappa^2 sin^2 \emptyset} \ d\emptyset \ . \tag{2.54}$$

This is evaluated from $0\ to\ \frac{\pi}{2}$ using a Maclaurin series expansion (see Weigel, 1960 for full details).

The expression for the free surface in time and space is:

$$y_S = y_t + Hcn^2\left[2K(\kappa)\left(\frac{x}{L}-\frac{t}{T}\right),\kappa\right] . \tag{2.55}$$

And the horizontal particle velocity is given as:

$$\frac{u}{\sqrt{gh_s}} = -\frac{5}{4}+\frac{3y_t}{2h_s}-\frac{y_t^2}{4h_s^2}+\left(\frac{3H}{2h_s}-\frac{y_tH}{2h_s^2}\right)cn^2\Theta-\frac{H^2}{4h_s^2}\,cn^4\Theta + \frac{8HK^2(\kappa)}{L^2}\left(\frac{h_s}{3}-\frac{y^2}{2h_s}\right)(sn^2\Theta\,dn^2\Theta-cn^2\Theta\,dn^2+\kappa^2cn^2\Theta\,sn^2) , \tag{2.56}$$

where the wavelength and trough elevation are defined respectively as:

$$L = \sqrt{\frac{16h_s^3}{3H}}\kappa\,K(\kappa) , \tag{2.57}$$

and

$$y_t = h_s - H + \frac{16h_s^3}{3L^2}\,\kappa\,K(\kappa)[K(\kappa)-E(\kappa)] . \tag{2.58}$$

To determine the elliptic modulus it is first necessary to state two definitions for wave celerity. Stokes' (1880) first definition of celerity from an Eulerian frame of reference, where to the fixed observer the particle velocity at any point below the trough is zero, given as:

$$\frac{C^2}{gh_s} = 1+\frac{H}{h_s}\left[-1+\frac{1}{\kappa^2}\left(2-3\,\frac{E(\kappa)}{K(\kappa)}\right)\right] . \tag{2.59}$$

However, by definition:

$$C = L/T , \tag{2.60}$$

And substituting for wavelength from Equation 2.57, the celerity can be expressed as:

$$C = \sqrt{\frac{16h_s^3}{3H}}\frac{\kappa\,K(\kappa)}{T} , \tag{2.61}$$

and thus

$$\frac{C^2}{gh_s} = \frac{16h_s^2}{3HT^2}\kappa^2 K^2(\kappa) \ . \tag{2.62}$$

Substituting Equation 2.62 into Equation 2.60 and subtracting the right hand side from each side results in a transcendental equation in *κ:*

$$f(k) = \frac{16h_s^2}{3HT^2}\kappa^2 K^2(\kappa) - 1 - \frac{H}{h_s}\left[-1 + \frac{1}{\kappa^2}\left(2 - 3\,\frac{E(\kappa)}{K\kappa}\right)\right] = 0 \ , \tag{2.63}$$

κ can now be found using Newton-Raphson iteration. The value is often close to unity therefore an initial guess of $\kappa = 1\text{-}10^{-12}$ would be reasonable.

3 Numerical Solution of Integral Wave Evolution Equations

Sobey's integral wave evolution equations in 1D space in the *x*-coordinate are solved numerically using a central differencing scheme, coupled with a matrix inversion method to separate mixed derivatives. The scheme is then marched forward in time using Runge-Kutta fourth order (RK4) time integration. For contrast the numerical solution for the 1HD SWE is given in Appendix B, and which is notably shorter and considerably less complex.

3.1 Finite Difference Scheme

The 1D grid shown in Figure 3.1 denotes a spatial domain on the horizontal axis, with points equally spaced by Δx, bound from $i = 1$ to $imax$, and the temporal domain on the vertical axis, with grid points k, separated by equal time steps Δt.

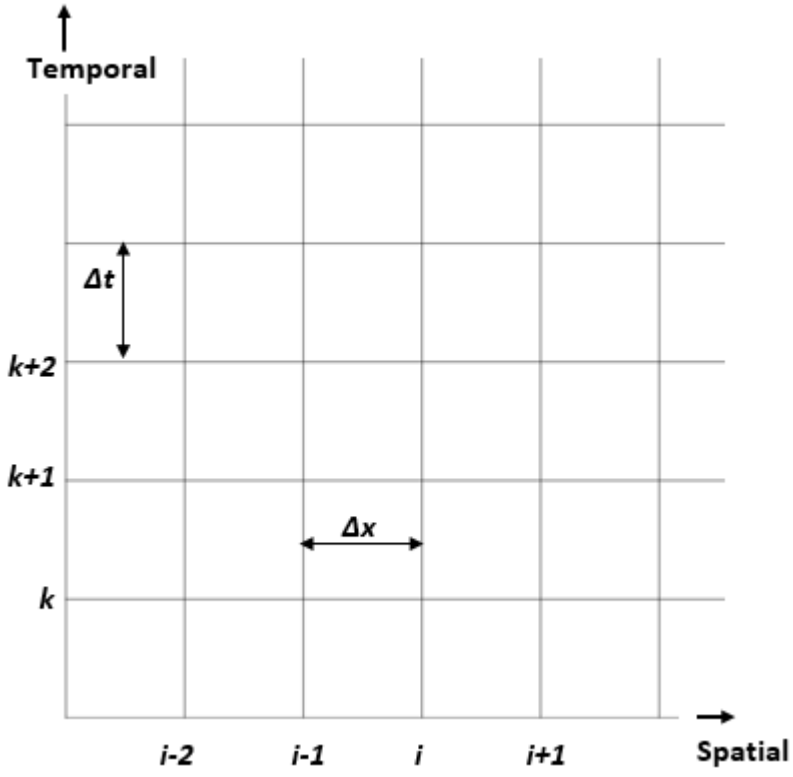

Figure 3.1. Finite difference grid with spatial steps on the horizontal axis and temporal steps on the vertical axis

To derive a central difference scheme Taylor series expansions are applied such that:

$$f(x_{i-1}) = f(x_i) - \frac{f'(x_i)}{1!}\Delta x + \frac{f''(x_i)}{2!}\Delta x^2 - \frac{f'''(x_i)}{3!}\Delta x^3 + \cdots , \tag{3.1}$$

and

$$f(x_{i+1}) = f(x_i) + \frac{f'(x_i)}{1!}\Delta x + \frac{f''(x_i)}{2!}\Delta x^2 + \frac{f'''(x_i)}{3!}\Delta x^3 + \cdots \tag{3.2}$$

Combining and rearranging gives

$$f'(x_i) = \frac{f(x_{i+1}) - f(x_{i-1})}{2\Delta x} - \frac{f'''(x_i)}{3!}\Delta x^2 + \cdots \tag{3.3}$$

Dropping the third order derivative gives:

$$f'(x_i) = \frac{f(x_{i+1}) - f(x_{i-1})}{2\Delta x} - O\Delta x^2 , \tag{3.4}$$

where $O\Delta x^2$ denotes that the scheme has been truncated to second-order accuracy for the first-order derivative.

The mass equation in 1HD is given as:

$$\frac{\partial \zeta}{\partial t} + \frac{\partial q}{\partial x} = 0 . \tag{3.5}$$

Rearranging and applying the differencing scheme, the temporal derivative can be expressed in terms of finite differences:

$$\frac{\partial \zeta}{\partial t}|_i^k = -\frac{q_{i+1}^k - q_{i-1}^k}{2\Delta x} . \tag{3.6}$$

The 1HD momentum equation (see Appendix A) is given by:

$$\frac{\partial q}{\partial t} + I_a\left[\frac{\partial}{\partial x}\left(\frac{q^2}{h}\right)\right] = -gh\frac{\partial \zeta}{\partial x} + \left(I_{p10}\frac{1}{2}h_s^2 + I_{p11}h_s\zeta\right)\left[\frac{\partial^2}{\partial x^2}\left(\frac{\partial q}{\partial t}\right)\right] + I_{p2}\frac{1}{2}h_s^2\left[\frac{\partial^2}{\partial x}\left(\frac{q}{h}\frac{\partial q}{\partial x}\right)\right] - \frac{\tau_{bx}}{\rho} . \tag{3.7}$$

Or, schematically

$$Term\ 1 + Term\ 2 = Term\ 3 + Term\ 4 + Term\ 5 + Term\ 6\ , \tag{3.8}$$

where,

$$Term\ 1 = \frac{\partial q}{\partial t}\ ,$$

$$Term\ 2 = I_a\left[\frac{\partial}{\partial x}\left(\frac{q^2}{h}\right)\right]\ ,$$

$$Term\ 3 = -gh\frac{\partial \zeta}{\partial x}\ ,$$

$$Term\ 4 = \left(I_{p10}\frac{1}{2}h_s^2 + I_{p11}h_s\zeta\right)\left[\frac{\partial^2}{\partial x^2}\left(\frac{\partial q}{\partial t}\right)\right]\ ,$$

$$Term\ 5 = I_{p2}\frac{1}{2}h_s^2\left[\frac{\partial^2}{\partial x}\left(\frac{q}{h}\frac{\partial q}{\partial x}\right)\right]\ ,$$

and

$$Term\ 5 = -\frac{\tau_{bx}}{\rho}\ .$$

.

Finite differences can be applied to *Terms 1, 2* and *3* with relative ease. However, *Terms 4* and *5* are complicated, especially *Term 4* which comprises both spatial and temporal derivatives. Therefore a separation method is sought. Moving terms containing temporal derivatives onto one side, Equation 3.7 can be re-written as:

$$\begin{aligned}\frac{\partial q}{\partial t} - \left(I_{p10}\frac{1}{2}h_s^2 + I_{p11}h_s\zeta\right)\left[\frac{\partial^2}{\partial x^2}\left(\frac{\partial q}{\partial t}\right)\right] &= -gh\frac{\partial \zeta}{\partial x} - I_a\left[\frac{\partial}{\partial x}\left(\frac{q^2}{h}\right)\right] \\ &+ I_{p2}\frac{1}{2}h_s^2\left[\frac{\partial^2}{\partial x}\left(\frac{q}{h}\frac{\partial q}{\partial x}\right)\right] - \frac{\tau_{bx}}{\rho}\ .\end{aligned} \tag{3.9}$$

Now let:

$$F = -gh\frac{\partial \zeta}{\partial x} - I_a\left[\frac{\partial}{\partial x}\left(\frac{q^2}{h}\right)\right] + I_{p2}\frac{1}{2}h_s^2\left[\frac{\partial^2}{\partial x}\left(\frac{q}{h}\frac{\partial q}{\partial x}\right)\right] - \frac{\tau_{bx}}{\rho}\ , \tag{3.10}$$

or, schematically:

$$F = \mathrm{T}erm\ 2 + \mathrm{T}erm\ 3 + \mathrm{T}erm\ 5 + \mathrm{T}erm\ 6\ , \tag{3.11}$$

which defines *F* in terms of spatial derivatives. However, by definition:

$$F = \frac{\partial q}{\partial t} - \left(I_{p10}\frac{1}{2}h_s^2 + I_{p11}h_s\zeta\right)\left[\frac{\partial^2}{\partial x^2}\left(\frac{\partial q}{\partial t}\right)\right], \tag{3.12}$$

which defines *F* in terms of temporal derivatives. Now let $\hat{q} = \frac{\partial q}{\partial t}$, and so Equation 3.12 is expressed as:

$$F = \hat{q} - \left(I_{p10}\frac{1}{2}h_s^2 + I_{p11}h_s\zeta\right)\left[\frac{\partial^2 \hat{q}}{\partial x^2}\right]\ , \tag{3.13}$$

or, schematically:

$$F = Term\ 1 + Term\ 4\ . \tag{3.14}$$

It is now possible to approximate both definitions for *F* in terms of finite differences and solve for $\hat{q}$ by setting up a tridiagonal system of equations. Applying differences to the first definition for *F* given by Equation 3.10 (or Equation 3.11 schematically):

$$\mathrm{Term}\ 2 = -gh_i\frac{\zeta_{i+1} - \zeta_{i-1}}{2\Delta x}\ , \tag{3.15}$$

$$Term\ 3 = -I_a\frac{\frac{q_{i+1}^2}{h_{i+1}} - \frac{q_{i-1}^2}{h_{i-1}}}{2\Delta x}\ , \tag{3.16}$$

and

$$Term\ 6 = \frac{\tau_{bxi}}{\rho}\ . \tag{3.17}$$

Term 5 contains multiplied derivatives which need to be separated using the chain rule, for which the first derivative is defined as:

$$\frac{\partial}{\partial x}(f.g) = f\frac{\partial g}{\partial x} + g\frac{\partial f}{\partial x}\ . \tag{3.18}$$

The second derivative is defined as:

$$\frac{\partial^2}{\partial x^2}(f.g) = \frac{\partial}{\partial x}\left(f\frac{\partial g}{\partial x} + g\frac{\partial f}{\partial x}\right) = g\frac{\partial^2 f}{\partial x^2} + 2\frac{\partial f}{\partial x}\frac{\partial g}{\partial x} + f\frac{\partial^2 g}{\partial x^2}\ . \tag{3.19}$$

Term 5 is then separated into three components:

$$I_{p2}\frac{1}{2}h_s^2\left[\frac{\partial^2}{\partial x}\left(\frac{q}{h}\frac{\partial q}{\partial x}\right)\right] = I_{p2}\frac{1}{2}h_s^2\left[\frac{\partial q}{\partial x}\frac{\partial^2\left(\frac{q}{h}\right)}{\partial x^2} + 2\frac{\partial^2 q}{\partial x^2}\frac{\partial\left(\frac{q}{h}\right)}{\partial x} + \frac{\partial^3 q}{\partial x^3}\frac{q}{h}\right]. \tag{3.20}$$

The components are a combination of first, second and third derivatives. Applying the differencing scheme, *Term 5* becomes:

$$I_{p2}\frac{1}{2}h_{si}^2\left[\left(\frac{q_{i+1} - q_{i-1}}{2\Delta x}\right)\left(\frac{\frac{q_{i+1}^2}{h_{i+1}} - 2\frac{q_i^2}{h_i} + \frac{q_{i-1}^2}{h_{i-1}}}{\Delta x^2}\right) + 2\left(\frac{q_{i+1} - 2q_i + q_{i-1}}{\Delta x^2}\right)\left(\frac{\frac{q_{i+1}}{h_{i+1}} - \frac{q_{i-1}}{h_{i-1}}}{2\Delta x}\right) + \frac{q_i}{h_i}\left(\frac{q_{i+2} - 2q_{i+1} + 2q_{i-1} + q_{i-2}}{2\Delta x^3}\right)\right].$$

The scheme now contains two nodes outside of the domain in terms of flux as a consequence of the third derivative component in *Term 5*, which will require additional boundary conditions. Now applying the differencing scheme to the second definition for *F* (Equation 3.13):

$$\mathrm{F}|_i^k = \widehat{q_i} - \left(I_{p10}\frac{1}{2}h_s^2 + I_{p11}h_s\zeta_i\right)\left(\frac{\hat{q}_{i+1} - 2\hat{q}_i + \hat{q}_{i-1}}{\Delta x^2}\right). \tag{3.21}$$

Now let:

$$I_i = \left(I_{p10}\frac{1}{2}h_s^2 + I_{p11}h_s\zeta_i\right), \tag{3.22}$$

then

$$\mathrm{F}|_i^k = \widehat{q_i} - I_i\left(\frac{\hat{q}_{i+1} - 2\hat{q}_i + \hat{q}_{i-1}}{\Delta x^2}\right), \tag{3.23}$$

Separating terms:

$$\mathrm{F}|_i^k = -\frac{I_i}{\Delta x^2}\hat{q}_{i-1} + \left(1 + \frac{2I_i}{\Delta x^2}\right)\hat{q} - \frac{I_i}{\Delta x^2}\hat{q}_{i+1}\ , \tag{3.24}$$

which can be defined as:

$$\mathrm{F}|_i^k = a_i\hat{q}_{i-1} + b_i\hat{q} + c_i\hat{q}_{i+1} \ , \tag{3.25}$$

where:

$$a_i = -\frac{I_i}{\Delta x^2}, \qquad b_i = \left(1 + \frac{2I_i}{\Delta x^2}\right), \qquad c_i = -\frac{I_i}{\Delta x^2} \ .$$

The resulting matrix system is:

$$\begin{bmatrix} b_2 & c_2 & & & & & & & \\ a_3 & b_3 & c_3 & & & & & & \\ & a_4 & b_4 & c_4 & & & & & \\ & & . & . & . & & & & \\ & & & a_i & b_i & c_i & & & \\ & & & & . & . & & & \\ & & & & & . & . & & \\ & & & & & & a_{imax-2} & b_{imax-2} & c_{imax-2} \\ & & & & & & & a_{imax-1} & b_{imax-1} \end{bmatrix} \begin{bmatrix} \hat{q}_2 \\ \hat{q}_3 \\ \hat{q}_4 \\ . \\ \hat{q}_i \\ . \\ . \\ \hat{q}_{imax-2} \\ \hat{q}_{imax-1} \end{bmatrix} = \begin{bmatrix} F_2 - a_2\hat{q}_1 \\ F_3 \\ F_4 \\ . \\ F_i \\ . \\ . \\ F_{imax-2} \\ F_{imax-1} - c_{imax-1}\hat{q}_{imax} \end{bmatrix}$$

(3.26)

noting that $\hat{q}_1$and $\hat{q}_{\mathrm{imax}}$ are prescribed boundary conditions.

The temporal flux derivatives are solved using the Thomas algorithm. First a forward sweep is carried out, decomposing terms to eliminate all a_i columns, then using backwards substitution the solution is obtained.

3.2 Time Integration

At the end of each spatial iteration, the rate of change is determined by marching the solution forward in time, a process which needs to be treated with due care. The Courant number (or CFL number) given by:

$$C = \frac{u_{max}\,\Delta t}{\Delta x} \tag{3.27}$$

is a measure of stability. For $C > 1$ instability may arise (Mitchell and Griffiths, 1980). Three time integration methods were investigated for stability and efficiency using a simple SWE solver (see Appendix B) to model channel flow with a uniformly increasing depth for which an analytical solution is known. The conditions required to arrive at an exact solution for velocity are shown in Table 3.1.

Table 3.1. Courant condition required for Euler, Adams-Bashforth, and Runge-Kutta time integration methods to arrive at the exact solution to uniform channel flow velocity, where u_{max} is 7.67 m/s and Δx is 10 m.

Method	**Δt (s)**	**Courant no.**
Euler	0.01	0.008
AB	0.1	0.077
RK4	2.8	2.148

The first order Euler approximation was found to be too unstable, the second order Adams-Bashforth method greatly improved the efficiency. However RK4 shows a vast improvement over both, giving an exact solution well outside of the Courant stability region. Thus to preserve the integrity of the proposed model the RK4 method is used. The RK4 algorithm is given as:

$$\zeta_i^{k+1} = \zeta_i^k + \frac{1}{6}\Delta t(k^1 + 2k^2 + 2k^3 + k^4)\,, \tag{3.28}$$

and

$$q_i^{k+1} = q_i^k + \frac{1}{6}\Delta t(k^1 + 2k^2 + 2k^3 + k^4)\,, \tag{3.29}$$

Where Equation 3.28 and Equation 3.29 give the new values for ζ and q. Hence k^1 is the slope at the beginning of the step given as:

$$k^1 = \left(\zeta_i^k, q_i^k\right) \tag{3.30}$$

where k^2 is the slope at the midpoint given in terms of Euler's formula using k^1:

$$k^2 = (\zeta_i^k + \frac{1}{2}\Delta t k^1, q_i^k + \frac{1}{2}\Delta t k^1) \tag{3.31}$$

where k^3 again uses Euler's formula with the definition for k^2 such that:

$$k^3 = \left(\zeta_i^k + \frac{1}{2}\Delta t k^2, q_i^k + \frac{1}{2}\Delta t k^2\right)\,. \tag{3.32}$$

k^4 is the final step which calculates the slope at the end based on k^3:

$$k^4 = \left(\zeta_i^k + \Delta t k^3, q_i^k + \Delta t k^3\right). \tag{3.1}$$

Thus RK4 gives a weighted estimate of four slopes over time using Simpson's rule.

3.3 Boundary Conditions

The boundary conditions applied were reflective at solid walls; and transmissive or radiation at open ends. Chapter 4 lists the free surface elevation and flux boundary conditions specified for each case. Where appropriate the initial conditions were ramped up with time from a boundary.

3.4 Shape Factors

The shape factors are an integral part of the model as they correct phase resolution. Sobey provides tables for each shape factor I_a, I_{p10}, I_{p11}, I_{p2}, (see Tables 4-7; Sobey, 2014). The factors are expressed as contours from two surfaces (previously introduced in Table 2.1): H/H_{Limit}, a measure of wave breaking which ranges from 0.01 – 0.80; and $\omega^2 h_s/g$, ranging from 0.02 - 4.00. Here H and ω are global estimates, which can be found from the wave spectra $E(\omega)$, such as the Pierson-Moskowitz spectrum given as:

$$E(\omega) = \frac{\alpha g^2}{\omega^5}\, e\left(-\beta \frac{\omega_0^4}{\omega^5}\right), \tag{3.34}$$

where, $\alpha = 0.0081$, $\beta = 0.74$, $\omega_0 = \frac{g}{U_c}$, and u_c the characteristic wind speed 19.5 m above the free surface. Other appropriate ocean spectra include, the JONSWOP, ISSC, and ITTC forms. A program which numerically models the spectra and matches significant wave heights and spectral frequencies is available (Borthwick, 2014). The program requires some manipulation before it can be introduced into the numerical model. One issue is that a characteristic wind speed is always required; the code requires amendment for application other than those generated by wind.

The spectral peak ω_p can be estimated from:

$$\omega_P = \frac{\int_0^\infty \omega E(\omega)^5 d\omega}{\int_0^\infty E(\omega)^5\, d\omega}. \tag{3.35}$$

And the wave height H_{rms} as:

$$H_{rms} = 2^{1.5} \int_0^{\infty} \omega E(\omega)\, d\omega \ . \tag{3.36}$$

This requires numerical integration which was beyond the brief of the present project. Instead, Sobey's tables are interpolated using cubic splines for later application.

4 Results and Discussion

In this chapter, three wave models are investigated: sloshing waves in a tank; progressive waves; and the dispersion of an initial mound (which includes harmonic analysis by decomposition).

4.1 Sloshing Waves

The first test for the numerical model is sloshing waves in a tank, which could represent waves reflecting off a harbour wall, or seiching in an ocean basin. The first order analytical solution (see; Lamb, 1932, Art 190, Dean and Dalrymple, 1991) gives a standing wave in space and time:

$$\zeta(x,t) = \frac{H}{2}\cos(kx)\cos(\omega t) \ , \tag{4.1}$$

where the wave number $k = 2\pi/L$. A higher order solution by Wei and Kirby (1995) involves solving and summing up all modes of oscillation. The domain stretches from $x = 0$, to $x = L$, with $h_s = 2\ m$. The initial condition at t = 0 s is given by Equation 4.1, where $H = h_s/50$, $L = 1000\ m$, *and* $\Delta x = 0.5\ m$. Reflective boundary conditions are applied at the wall where $q = 0$, and ζ is determined by linear extrapolation.

An initial attempt to model, Sobey's wave (II) given in Table 2.1, where [I_a, I_{p10}, I_{p11}, I_{p2}] = [1.024, 1.045, -0.563, 0.910], became unstable because sloshing waves are of a non-dispersive nature. Correcting for this, but without reverting to SWE conditions ([I_a, I_{p10}, I_{p11}, I_{p2}] = [1, 0, 0, 0]). Figure 4.1 shows the non-dimensional time history of the free surface elevation obtained when the advective dispersive component was omitted from wave (*II*) ($I_{p2} = 0$) to account for stationary nodes. Although this correction appeared to work until $\frac{t}{T} \sim 2.5$, the wave became unstable by $\frac{t}{T} \sim 4$, with the back face shocking up and becoming ever steeper. The next step was to investigate the effect of the I_{p11} shape factor since this multiplies a highly non-linear term $(I_{p11}h_s\zeta)$ which in turn multiplies the mixed derivative. The sign was first swapped, and as shown in Figure 4.2 this amendment reversed the direction of the shock to be more consistent with waves breaking (assuming left to right propagation). The front face is becoming steeper, the velocity is increasing to the point where the wave breaks (and particles would jump off), but in the absence of a shock-capturing scheme, the numerical model begins to break down as would be expected. Next the magnitude of I_{p11} was decreased to 0.1 leading to the results shown in Figure 4.3. This removes shocking and improves stability, with the model able to cope with a Courant number twice as large. There is still a very slight slant to the right.

Removing the term altogether as shown in Figure 4.4, removes the slant. This is in good agreement with the analytical solution (Figure 4.5), and exactly matches the results from the SWE model (Figure 4.6) which incidentally is far more stable, managing a Courant number of 1.772.

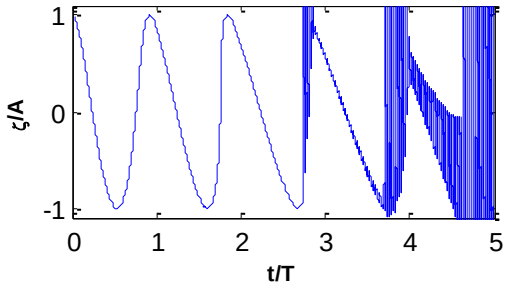

Figure 4.1. Ip2 = - 0.563, C = 0.044

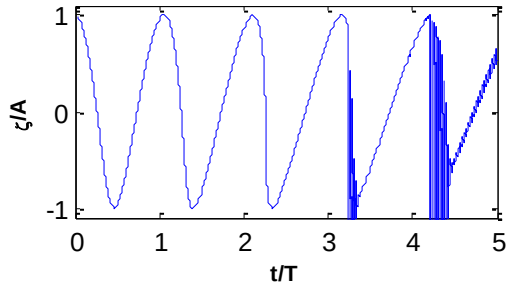

Figure 4.2 Ip2 = 0.563, C = 0.044

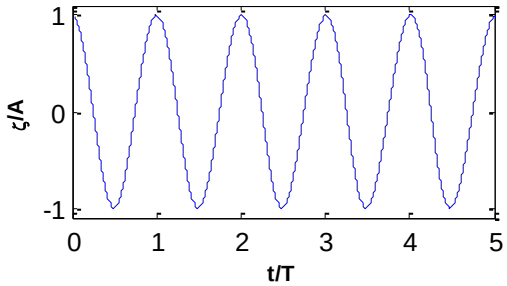

Figure 4.3. Ip2 = 0.1, C = 0.089

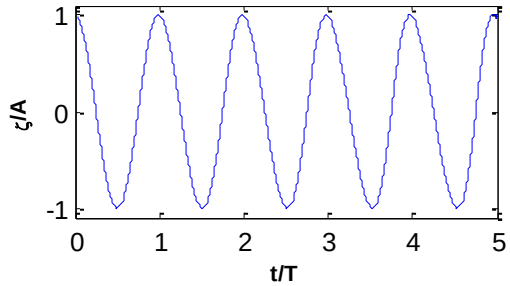

Figure 4.4. Ip2 = 0, C = 0.089

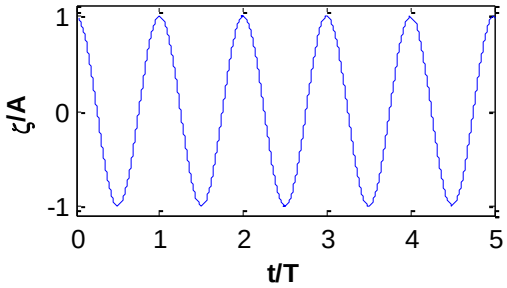

Figure 4.5. Analytical solution

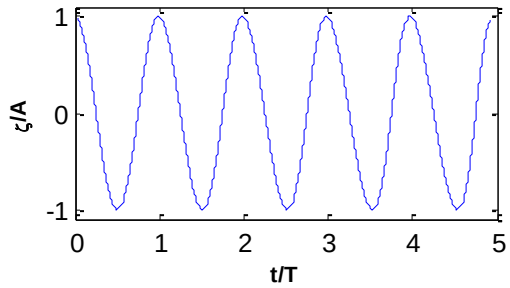

Figure 4.6. Shallow water model: C = 1.772

4.2 Evolution of Progressive Waves

An attempt was made to model progressive waves. The initial conditions for the free surface and local flux determined from cnoidal theory are shown in Figure 4.7 and Figure 4.8 respectively, where $T = 10$ *s*, $h_s = 2$ *m*, $H = 0.5$ *m*, with corresponding wavelength L = 46.5 m. However the model quickly became unstable. The wave was gradually introduced into the model using a ramping function at the boundary x= 0 m with reflective conditions at the far wall. The rates of change at the boundary were determined by passing the boundary values through a second finite difference scheme. The increased complexity raised concerns, at which point

a simple non-linear wave was passed into the system in a similar manner, but again the system quickly became unstable again. It is believed that the instability arose from the central differencing of the non-linear terms in the governing equations. In future, an enhanced scheme based on upwind difference is recommended.

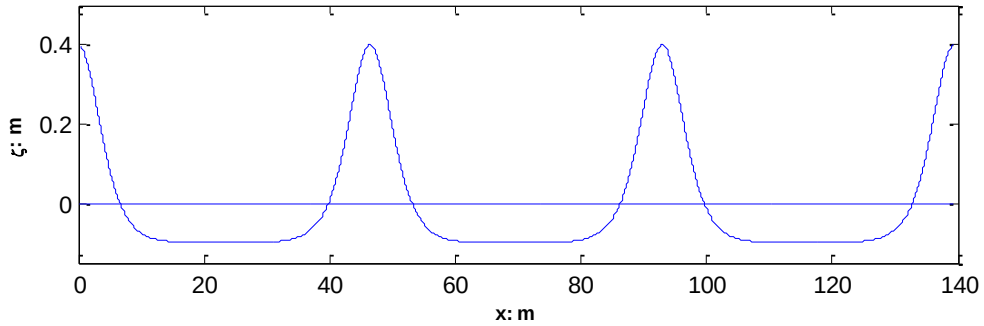

Figure 4.7. Initial free surface elevation conditions given by cnoidal wave theory

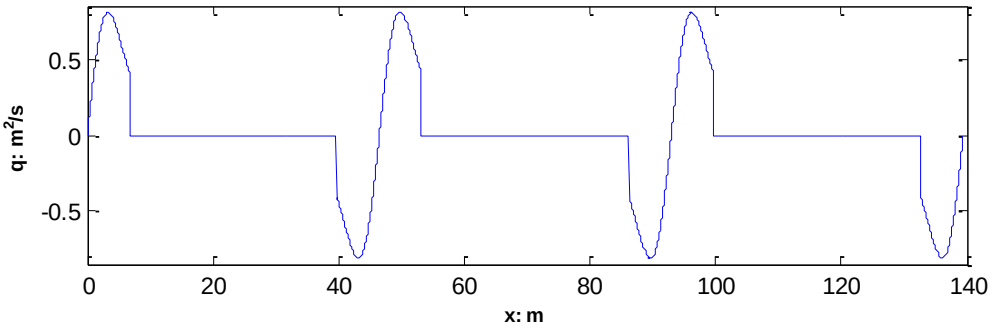

Figure 4.8. Initial flux conditions given by cnoidal wave theory

4.3 Dispersion of an Initial Mound

To validate the dispersive and transient properties of the model the free surface motion introduced by the release of an initial mound from rest are investigated. The linear solution to this Cauchy-Poisson problem is a Fourier transform in space over an infinite depth (Lamb, 1932 Art 238), which is extended into finite depth (Sobey, 2014). The analytical solution requiring numerical integration is not pursued due to time constraints. The investigation proceeds by validation of the model with that of Sobey. Then an investigation into the ability of the solver to capture non-linear behaviour is performed. The initial conditions are *q(x,0)* = 0, and $\zeta(x,0) = \zeta(x)$ at *t* = 0 s, given by a Gaussian hump centred at *x* = 0, as shown in Figure 4.9a:

$$\zeta(x) = Ae[-\ln 2\,(x/b)^2] \ . \tag{4.2}$$

We first consider the case of a relatively steep Gaussian hump (*A* = 5 m, *b* = 50 m) where the waves released with travel in water of still water depth (h_s = 100 m) correspond to deep to

intermediate depth waves following Sobey (2014). Here the shape factors are: [I_a, I_{p10}, I_{p11}, I_{p2}] = [1.01, 0.64, 0.34, 1]. The results presented in Figure 4.9, show that the free surface profiles at times t = 0, 5, 15 and 30 s are symmetrical about the origin where the flux is antisymmetric, validating the model. The initial mound takes over 15 s to fall to the free surface, which is much longer than Sobey's model suggesting that there is a problem in the finite difference scheme with temporal advective dispersion.

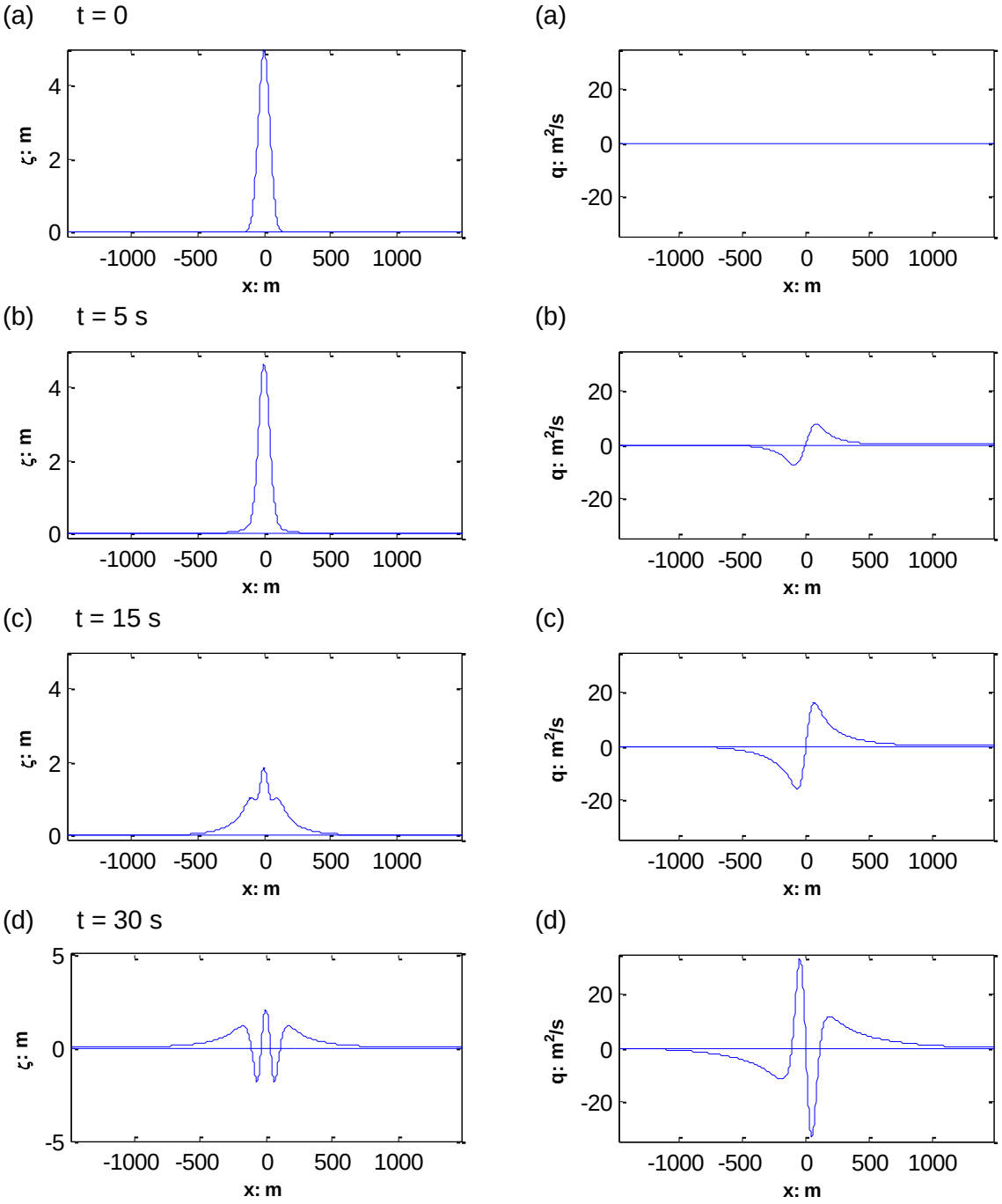

Figure 4.9. Deep water Cauchy-Poisson problem spatial profile of free surface and corresponding flux, for initial conditions, t = 5, 15 and 30 s

Harmonic analysis of two symmetrical disturbances is now investigated using superposition. A similar method has previously been applied to focused waves in shallow water (e.g. Borthwick et al., 2006b) and extreme ocean waves in deep water (e.g. Johannessen and Swan, 2001), but to the author's knowledge has of yet never been applied to the dispersion of an initial mound of water. The analysis gives insight into the non-linear behaviour by the separation of odd and even harmonics, since the odd harmonics contain linear, third-order and higher odd terms, and the even harmonics contain non-linear second order terms (Borthwick et al., 2006b). The approach involves simulating two initially symmetrical cases: a crest hump (ζ_C), and trough hump (ζ_T). The initial conditions for each are the Gaussian hump, with a negative amplitude for the trough. The even harmonics (ζ_{Even}) are then given by:

$$\zeta_{Even} = \frac{\zeta_C + \zeta_T}{2} \ . \tag{4.3}$$

With the odd harmonics(ζ_{Odd}) determined by:

$$\zeta_{Odd} = \frac{\zeta_C - \zeta_T}{2} \ . \tag{4.4}$$

For a linear wave the wave profile of the even harmonics should be zero with no disturbances about the SWL. However, the greater the amplitude of the initial hump the more pronounced the non-linearity leading to the presence of second, even and higher order harmonics. For the linear wave case, the first-order odd (subtracted) harmonic profile should exactly match the crest hump profile.

The first test involves a hump of moderate steepness (A = 0.5 m, b = 30 m, L = 1500 m, h_s = 30 m, Δx = 2.14 m, Δt = 0.1 s), with initial conditions shown in Figure 4.10. Figure 4.11 through to Figure 4.14 present spatial profiles for crest, trough, odd and even harmonics, at t = 5, 15, 30, and 60 s, respectively. The initial condition is linear, but over time the hump splits up releasing non-linear components. Although the magnitudes of the even and odd harmonics are similar to begin with, the even harmonics decay quicker than the odd with time. This suggests that there is considerable non-linear behaviour within the dispersion of the mound, which is in agreement with theory, referring back to the Ursell parameter (Equation 1.1). The results validate the solver's ability to model higher-order terms. The time series and corresponding single-sided frequency spectra are compared for both harmonics (shown in Figure 4.15) at x = 0. This shows that the dispersion is dominated by a single peak frequency of about 0.065 Hz, with period 15.38 s, which by analogy of simple harmonic motion involving a length scale divided by gravity (with the appropriate length scale approximated by the width of the mound) gives:

$$T = 2\pi\sqrt{\frac{2b}{g}} = 15.39\ s\ . \tag{4.5}$$

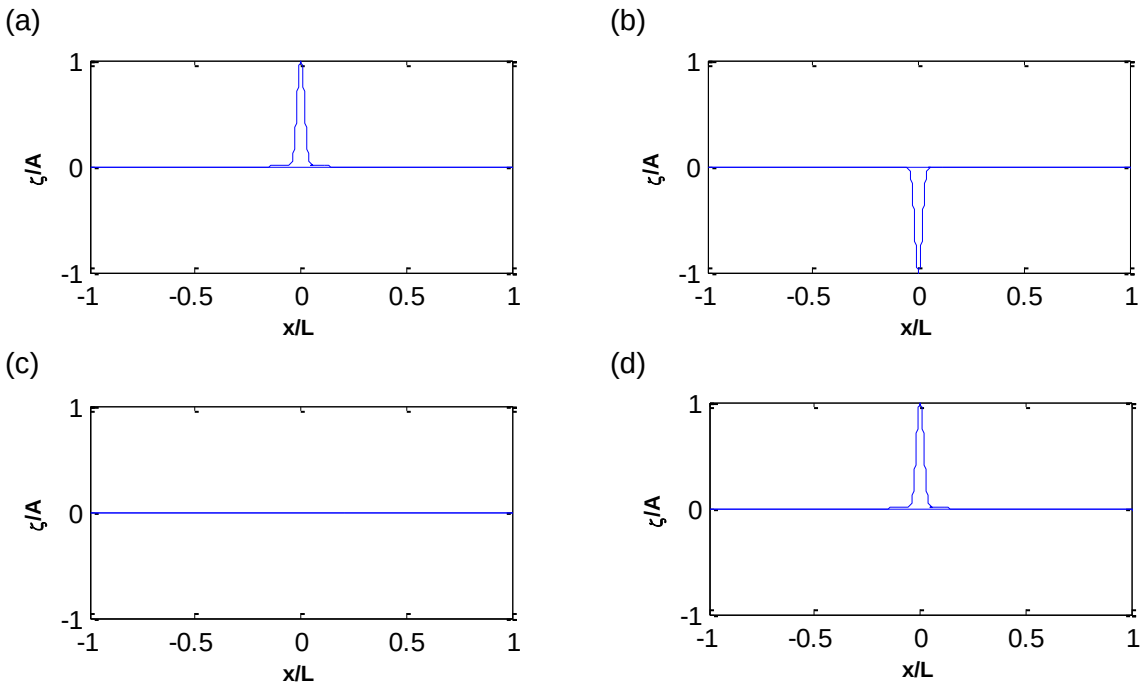

Figure 4.10. Spatial profile of free surface elevation initial conditions at t = 0 s for (a) crest, (b) trough, (c) even harmonics, and (d) odd harmonics

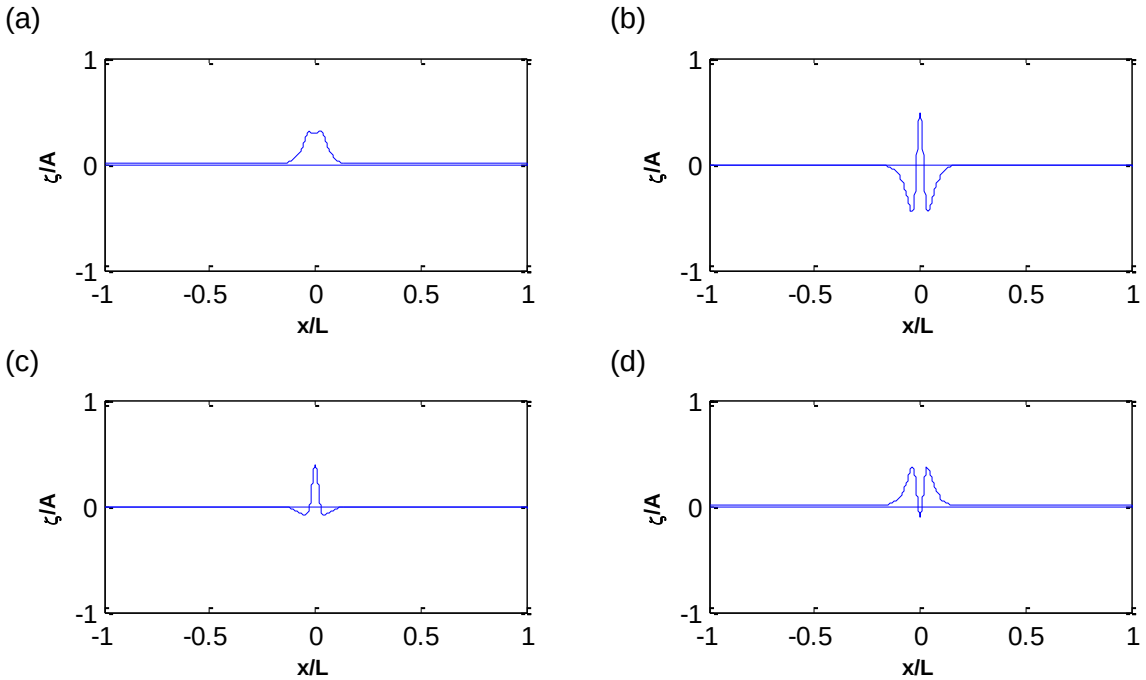

Figure 4.11. Spatial profiles of free surface elevation at t = 5 s for (a) crest, (b) trough, (c) even harmonics, and (d) odd harmonics

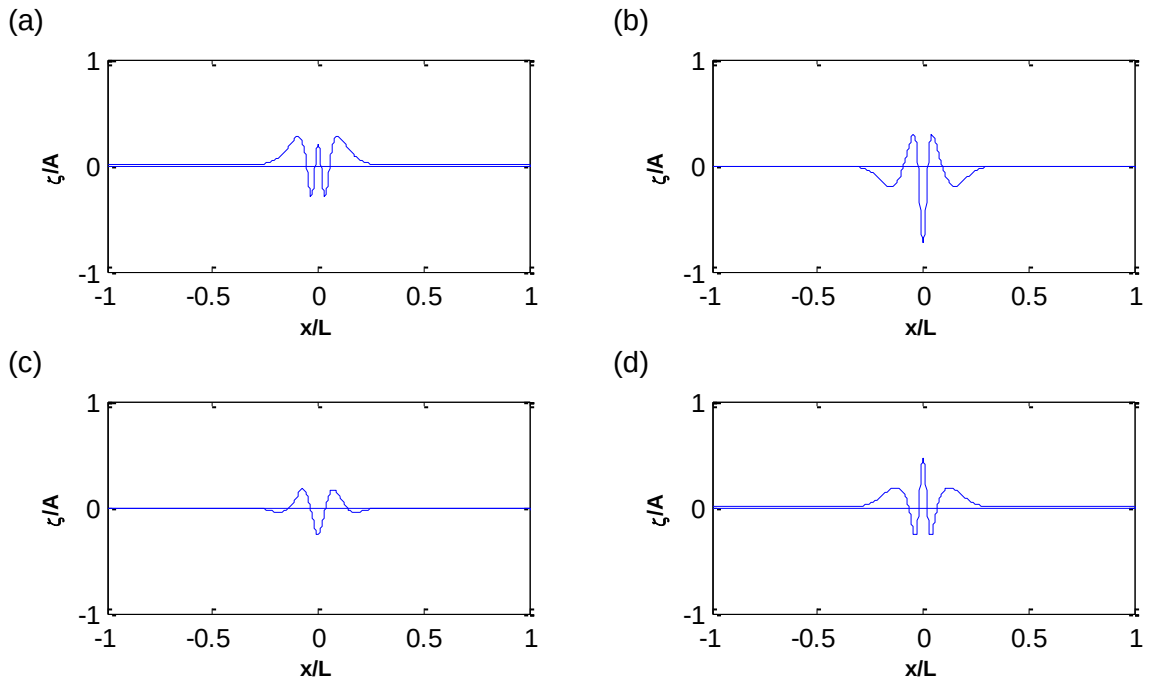

Figure 4.12. Spatial profiles of free surface elevation at t = 15 s for (a) crest, (b) trough, (c) even harmonics, and (d) odd harmonics

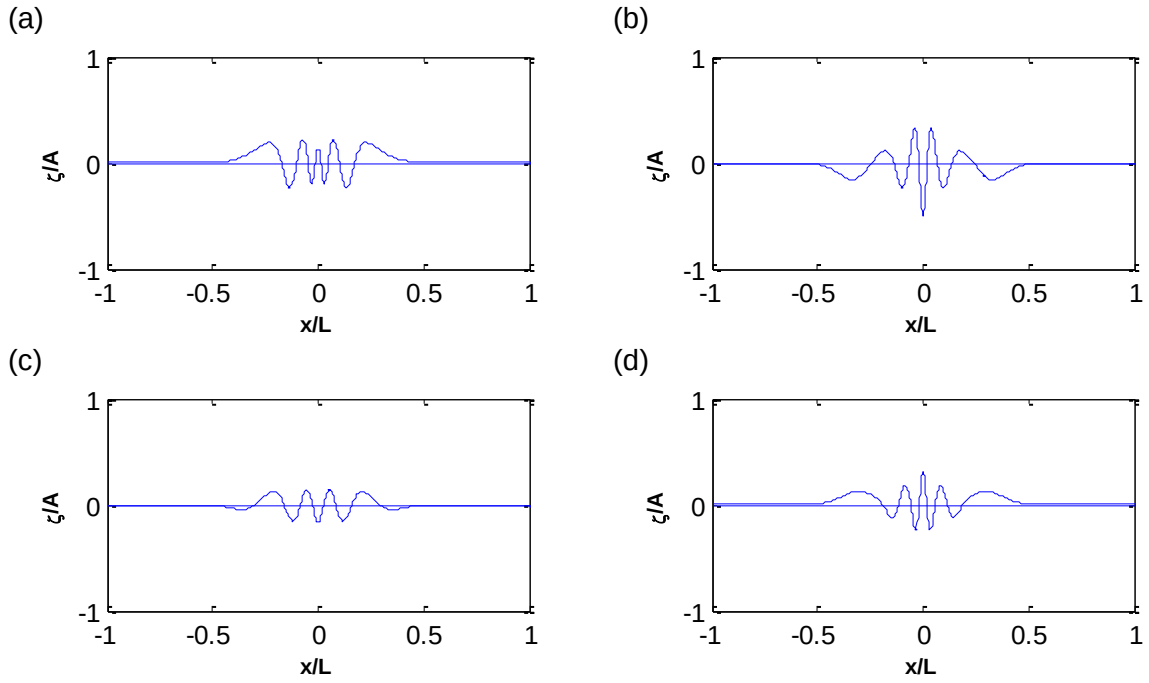

Figure 4.13. Spatial profiles of free surface elevation at t = 30 s for (a) crest, (b) trough, (c) even harmonics, and (d) odd harmonics

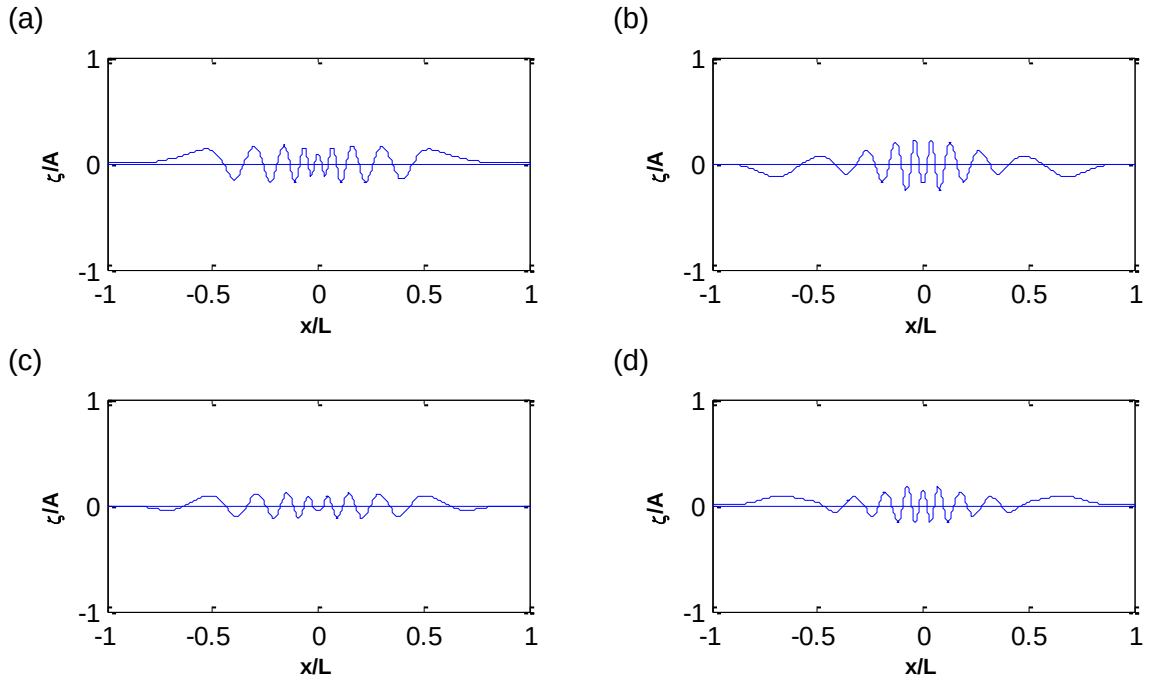

Figure 4.14. Spatial profiles of free surface elevation at t = 60 s for (a) crest, (b) trough, (c) even harmonics, and (d) odd harmonics

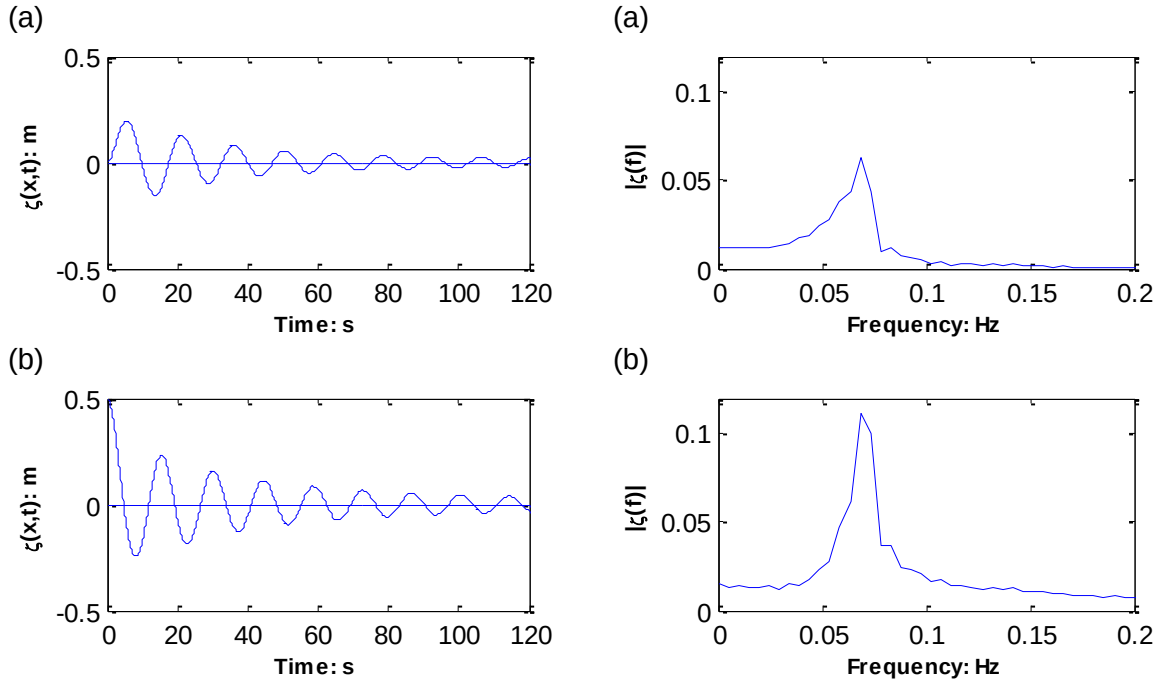

Figure 4.15. Time series and resulting frequency spectra for (a) even harmonics, and (b) odd harmonics at x = 0

The next test involves a hump of gentle steepness (A = 0.1 m, b = 30 m, L = 1500 m, h_s = 30 m, Δx =2.14 m, Δt = 0.1 s), with initial conditions shown in Figure 4.16. Figure 4.17 through to Figure 4.20 show spatial profiles of the crest, trough, odd and even harmonics, at t = 5, 15, 30, and 60 s, respectively. Again the initial conditions are linear. At 5 s there is a small even-

harmonic profile, which becomes negligible as the mound decays. In addition the spatial profile of the odd harmonics closely resemble the crest at each interval. Thus the solver does not simulate non-linear wave components in agreement with small-amplitude (linear) wave theory.

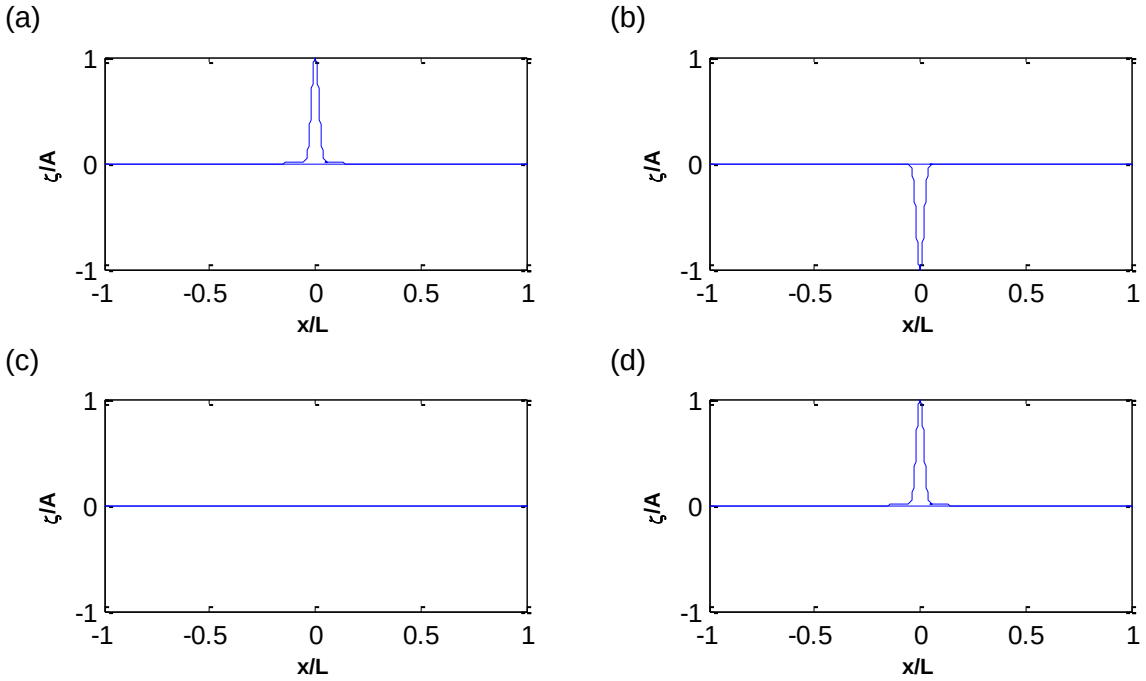

Figure 4.16. Spatial profile of initial conditions of smaller hump at t = 0 s for (a) crest, (b) trough, (c) even harmonics, and (d) odd harmonics

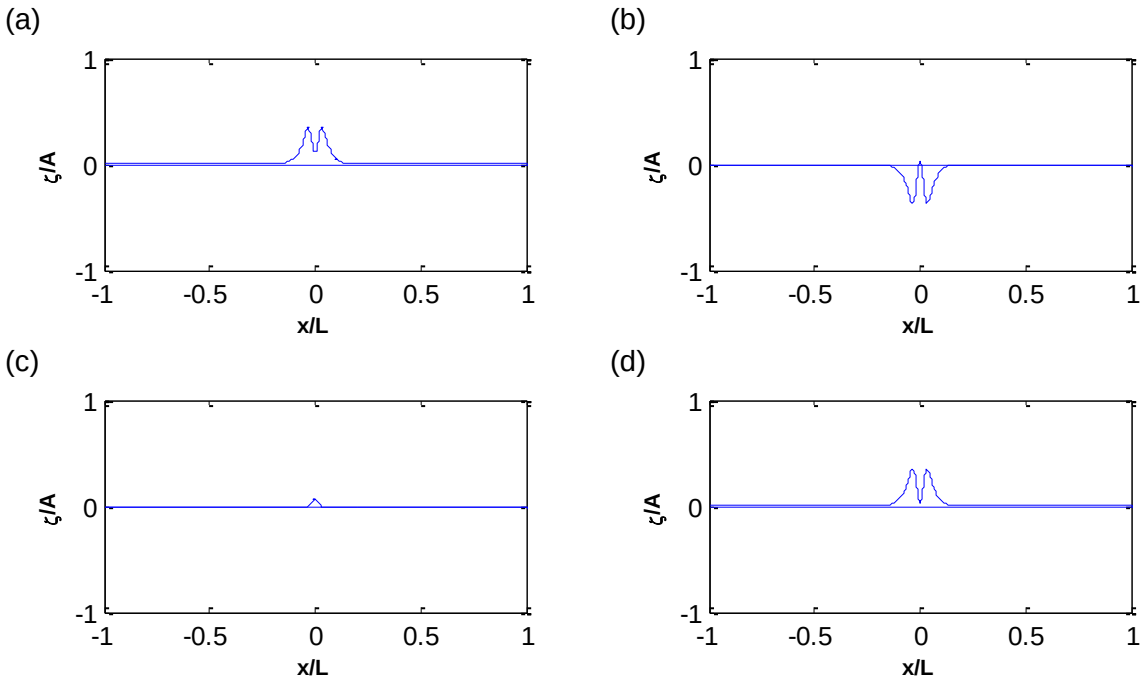

Figure 4.17. Spatial free surface profiles of smaller initial hump at t = 5 s for (a) crest, (b) trough, (c) even harmonics, and (d) odd harmonics

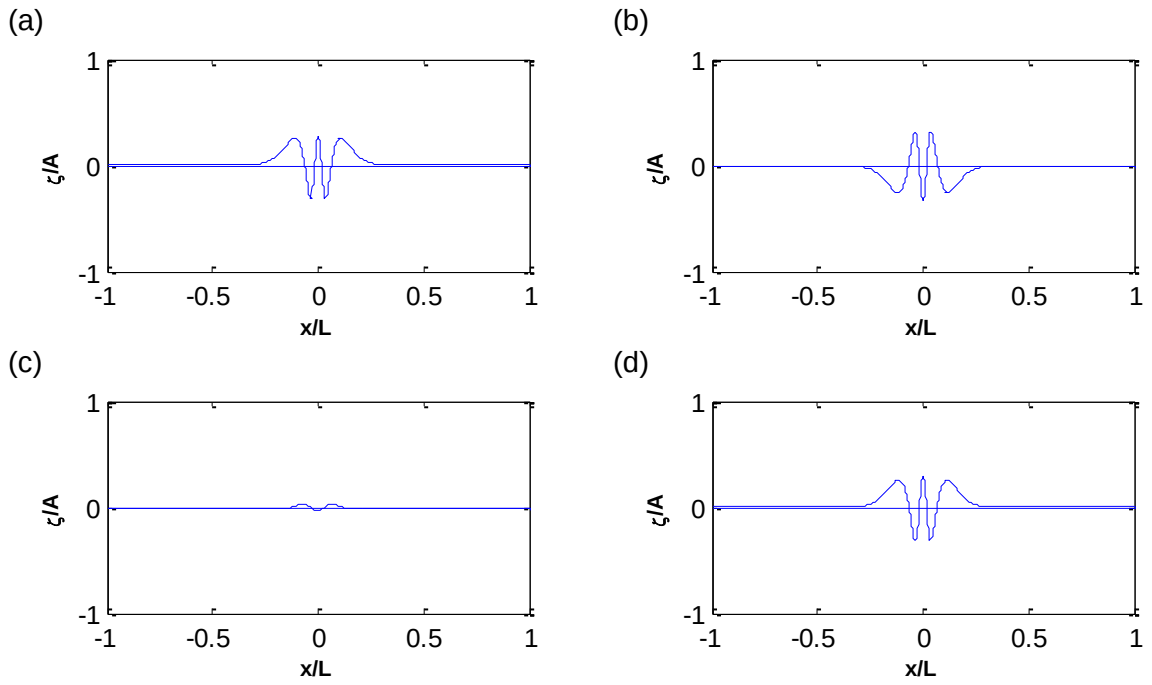

Figure 4.18. Spatial free surface profiles of smaller initial hump t = 15 s for (a) crest, (b) trough, (c) even harmonics, and (d) odd harmonics

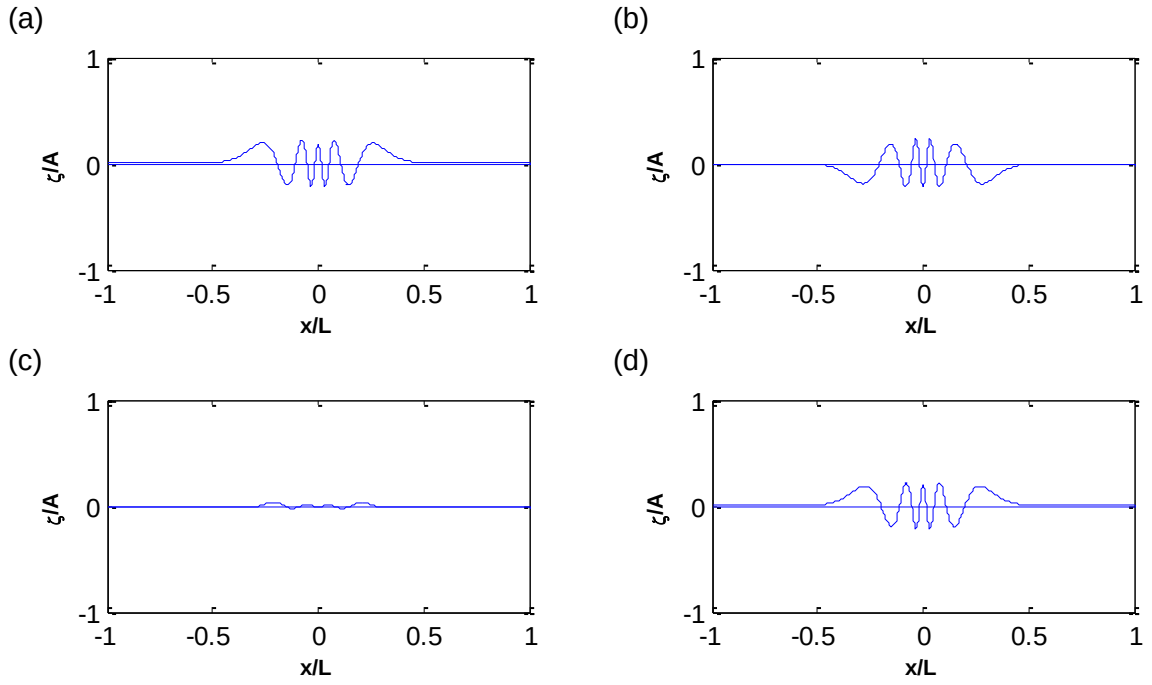

Figure 4.19. Spatial free surface profiles of smaller initial hump t = 30 s for (a) crest, (b) trough, (c) even harmonics, and (d) odd harmonics

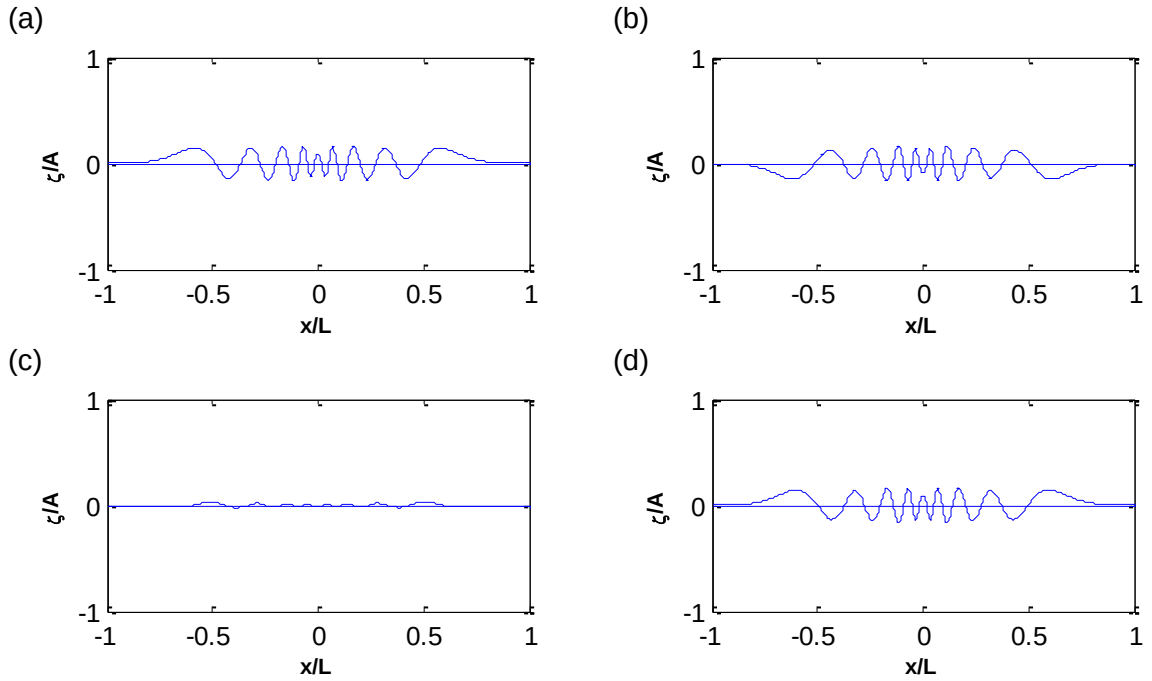

Figure 4.20. Spatial free surface profiles of smaller initial hump t = 60 s for (a) crest, (b) trough, (c) even harmonics, and (d) odd harmonics

The final test concerns the effect of turning off the l_{p11} term and introducing large amplitude waves. Figure 4.21 and Figure 4.22 show spatial profiles at t = 60 s for initial amplitudes of 3 and 1 m respectively.

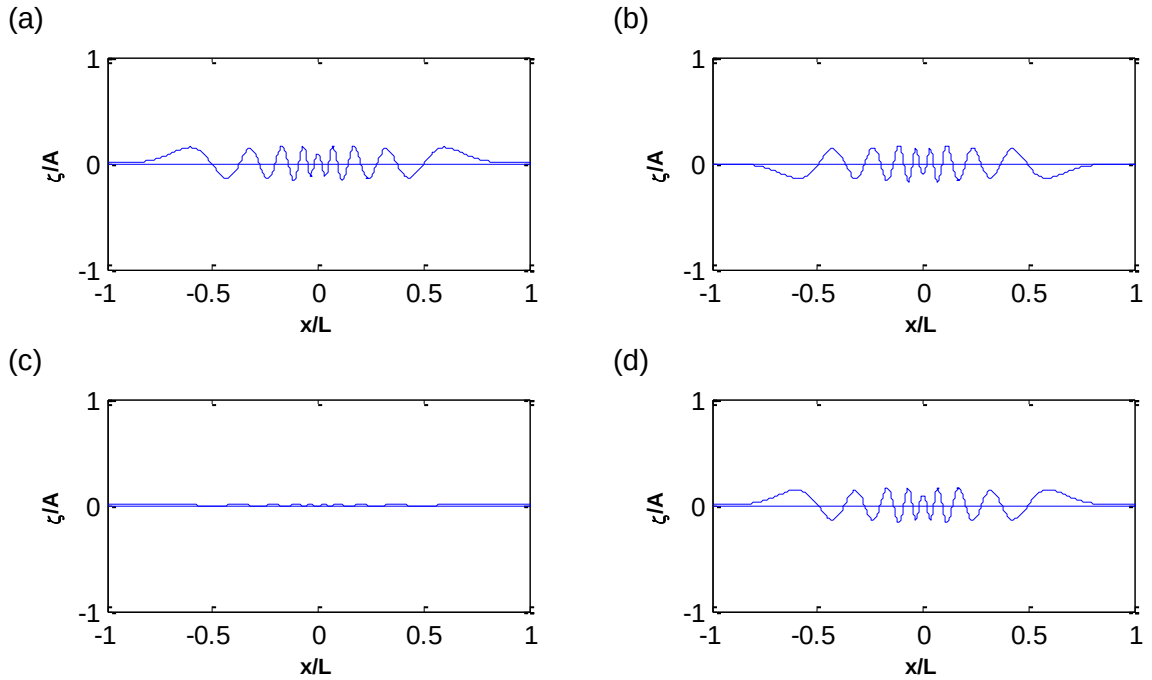

Figure 4.21. Spatial free surface profiles for a Gaussian hump initial amplitude of 3 m, at t = 60 s for (a) crest, (b) trough, (c) even harmonics, and (d) odd harmonics

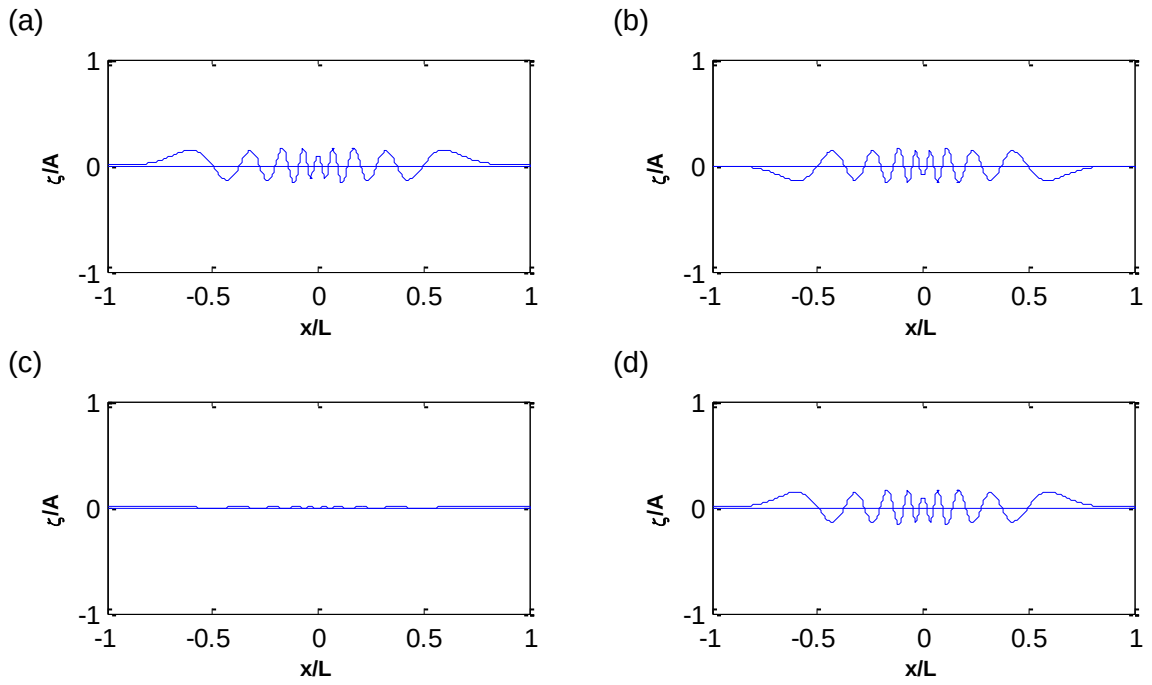

Figure 4.22. Spatial free surface profiles for a Gaussian hump initial amplitude of 1 m, at t = 60 s for (a) crest, (b) trough, (c) even harmonics, and (d) odd harmonics

With the l_{p11} term off, the solver is stable enough to model the higher amplitude hump cases, but what is apparent from the even-harmonic profiles is the failure to capture non-linear behaviour, which is incorrect. Moreover there seems to be hardly any difference in the profiles for the 3 and 1 m amplitudes, even though the 3 m amplitude is much steeper, thus the resulting kinetic energy of the flow should produce more waves over an equal period of time.

4.4 Discussion

The wave evolution tests have highlighted the sensitivity of the solver, especially with respect to the non-linear scale associated with l_{p11} which deals with the temporal advective dispersion, mixed derivative term. The results from sloshing show that hydrostatic waves can be modelled by switching off the dispersive terms, but this can be achieved more efficiently with a SWE solver. However, the ability to show incipient shock behaviour without a shock-capturing scheme is surprising, since the differencing scheme is not designed to deal with the extreme gradients. The mound test gave insight into the limits of the model. The deep water test case of Sobey did not disperse as quickly in time as would be expected. However, compared to Sobey's more advanced MOC model the fact that the present results extended into the range is encouraging. The harmonic analysis validated that the solver can model non-linear and weakly non-linear waves. Steeper humps could be modelled without the l_{p11} term. However,

non-linear terms were not captured. These results together with the inability to model progressive waves suggests that the model is limited by the simple-central differencing scheme used to discretise the temporal advective term.

5 Conclusions and Recommendations

This chapter lists the important findings and makes recommendations for future work.

5.1 Conclusions

- A numerical model for Sobey's phase-resolving integral equations has been developed using a central-differencing scheme.
- The model was tested for sloshing in a rectangular tank, progressive waves and the dispersion of an initial mound.
- Sloshing waves validated the model for hydrostatic waves, but highlighted a problem in discretising the dispersive terms in a central-difference scheme. With these terms switched off, the solution closely agrees with theory.
- Attempts to model progressive waves with initial conditions provided by cnoidal wave theory proved unsuccessful, again due to the discretisation of the dispersive terms.
- The dispersion of an initial mound test gave good insight into the ability and limits of the model.
- The model works very well for linear waves and reasonably well for moderate amplitude weakly non-linear waves, but is unstable for large amplitude highly non-linear tests.
- The nature of the equations needs further consideration. All terms bar one in the momentum equation are non-linear and so a more optimised numerical scheme is required to obtain accurate results over a larger range of cases.
- The results have shown that a simple finite differencing scheme has application even when applied to a highly non-linear set of equations.
- The model is limited by the central differencing scheme and requires this to be converted into an enhanced scheme capable of dealing with the temporal advective mixed derivative terms associated with the I_{p11} scaling factor.

5.2 Recommendations

It is strongly recommended that any future work proceeds by first implementing a higher-order differencing scheme, and that the temporal advective mixed derivative term especially is treated with an upwinding scheme to damp out instabilities in the model. Shock-capturing may be achieved using a Godunov-type finite volume scheme with a suitable approximate Riemann solver. Once the foregoing has been implemented, an investigation into how best to select shape factors for each model is required, Sobey selected the factors by comparison with high

order analytical solutions for progressive waves. Therefore correlating these to other wave models would be most useful. A parameter study would be beneficial to highlight further areas of possible enhancement. Then extension into 2HD to include the *y*-component is recommended. Then applying the model to realistic ocean waves and engineering problems. Some of which are: water-sediment and water-quality simulations; tidal turbine power extraction; wave run-up and overtopping at coastal infrastructure; and waves propagating in future sea levels provided by global warming scenarios.

References

ABBOTT, M. B. 1979. *Computational Hydraulics: Elements of the Theory of Free Surface Flows,* London, Pitman.

BERKHOFF, J. C. W. Computation of combined refraction-diffraction. Proceedings of 13th Conference on Coastal Engineering, 1973 1972 Vancouver, Canada. ASCE, 471-490.

BORTHWICK, A. G. L., FORD, M., WESTON, B. P., TAYLOR, P. H. & STANSBY, P. K. 2006a. Solitary wave transformation, breaking and run-up at a beach. *Maritime Engineering,* 159**,** 97-105.

BORTHWICK, A. G. L., HUNT, A. C., FENG, T., TAYLOR, P. H. & STANSBY, P. K. 2006b. Flow kinematics of focused wave groups on a planebeach in the U.K. Coastal Research Facility. *Coastal Engineering,* 53**,** 1033-1044.

BOYLE, G. 2004. *Renewable Energy: Power for a Sustainable Future,* Milton Keynes, Oxford University Press.

CHAMBERLAIN, P. G. & PORTER, D. 1995. The modified mild-slope equation. *Journal of Fluid Mechanics,* 291**,** 393-407.

DEAN, R. G. & DALRYMPLE, R. A. 1991. *Advanced Series in Ocean Engineering,* Singapore, World Scientific.

FALCONER, R. A. 1993. An introduction to nearly horizontal flows. *In:* ABBOTT, M. B. & PRICE, W. A. (eds.) *Coastal, Estuarial and Harbour Engineers' Reference Book.* London: E & FNSpon Ltd.

IWAGAKI, Y. Hyperbolic Waves and Their Shoaling. Proceedings of 11th Internation Conference in Coastal Engineering, 1968 London. 124-144.

JOHANNESSEN, T. B. & SWAN, C. A laboratory study of the focusing of transient and directionally spread surface water waves. Royal Society, 2001 London. 971-1006.

KEULEGAN, G. H. & PATTERSON, G. W. 1940. Mathematical theory of irrotational translation waves. *Research of the National Bureau of Standards,* 24**,** 47-101.

LAMB, H. 1932. *Hydrodynamics,* Cambridge, Cambridge University Press.

MADSEN, P. A. & SORENSEN, O. R. 1992. A new form of the Boussinesq equations with improved linear dispersion characteristics. Part 2. A slowly-varying bathymetry. *Coastal Engineering***,** 183–204.

MEHAUTE, B. L. 1976. *An introduction to hydrodynamics and water waves,* New York, Springer-Verlag.

MITCHELL, A. R. & GRIFFITHS, D. F. 1980. *The Finite Difference Method in Partial Differential Equations,* Chichester, John Wiley and Sons Ltd.

MUNK, W. H. Origin and generation of waves. Proceedings of the First Conference on Coastal Engineering, 1951 Long Beach. 1-4.

OLIVER-SMITH, A. 2009. Sea Level Rise and the Vulnerability of Coastal Peoples:Responding to the Local Challenges of Global Climate Change in the 21st Century. *UNU Institute for Environment and Human Security,* 7**,** 1-56.

ORSZAGHOVA, J., BORTHWICK, A. G. L. & TAYLOR, P. H. 2011. From the paddle to the beach – A Boussinesq shallow water numerical wave tank based on Madsen and Sørensen's equations. *Journal of Computational Physics,* 231**,** 328-344.

PEREGRINE, D. H. 1967. Long waves on a beach. *Journal of Fluid Mechanics,* 27**,** 815-827.

REEVE, D., CHADWICK, A. & FLEMING, C. 2004. *Coastal Engineering: Processes, Theory and Design Practice,* New York, Spon Press.

SOBEY, R. J. 2014. Phase-resolving integeral wave evolution in a coastal environment. *Engineering and Computational Mechanics,* 167**,** 167-194.

THORNE, C., EVANS, E. & PENNING-ROWSELL, E. 2007. *Future Flooding and Coastal Erosion Risks,* London, Thomas Telford Ltd.

TULLY, S. & INGRAM, D. 2014. Modelling Tidal Channels: Preliminary results in Turbulence. *Proceedings of Oceans 2014 MTS/IEEE Taipei, Taiwan.* IEEE.

URSELL, F. 1953. The long-wave paradox in the theory of gravity waves. *Mathematical Proceedings of the Cambridge Philosophical Society,* 49**,** 685 - 694.

WEI, G. & KIRBY, J. T. 1995. Time-dependent numerical code for extended Boussinesq equations. *Journal of Waterway, Port, Coastal, and Ocean Enineering,* 121**,** 251-261.

WEI, G., KIRBY, J. T., GRILLI, S. T. & SUBRAMANYA, R. 1995. A fully nonlinear Boussinesq model for surface waves. Part 1. Highly nonlinear unsteady waves. *Journal of Fluid Mechanics,,* 294**,** 71-92.

WIEGEL, R. L. 1960. A presentation of cnoidal wave theory for practical application. *Journal of Fluid Mechanics,* 7**,** 273-286.

Appendix A

The phase-resolved integral momentum equations in tensor form are:

$$\rho\frac{\partial q_\alpha}{\partial t}+\rho I_a\frac{\partial}{\partial x_\beta}\left(\frac{q_\alpha q_\beta}{h}\right)=-\rho g h\frac{\partial\zeta}{\partial x_\alpha}+\rho\left(I_{p10}\frac{1}{2}h_s^2+I_{p11}h_s\zeta\right)\frac{\partial}{\partial x_\alpha}\left(\frac{\partial^2 q_\beta}{\partial t\partial x_\beta}\right)$$
$$+\rho\, I_{p2}\frac{1}{2}h_s^2\,\frac{\partial^2}{\partial x_\alpha\partial x_\beta}\left(\frac{q_\beta}{h}\frac{\partial q_\gamma}{\partial x_\gamma}\right)+\sum w\alpha-\sum b\alpha \tag{7.1}$$

where $\alpha,\beta,and\ \gamma$ take the values 1, and 2.

Or, schematically:

$$term\ 1+term\ 2=\ term\ 3+term\ 4+term\ 5+term\ 6\ . \tag{7.2}$$

To determine the momentum equation in the *x*-coordinate $\alpha=1$, throughout.

Term 1 is simply:

$\alpha=1,$

$$\rho\frac{\partial q_\alpha}{\partial t}=\rho\frac{\partial q_1}{\partial t}\ . \tag{7.3}$$

Term 2 has β components, and is expanded for values 1, 2 as follows:

$\alpha=1,\beta=1,$

$$\rho I_a\frac{\partial}{\partial x_\beta}\left(\frac{q_\alpha q_\beta}{h}\right)=\rho\, I_a\left[\frac{\partial}{\partial x_1}\left(\frac{q_1^2}{h}\right)\right]\ , \tag{7.4}$$

$\alpha=1,\beta=2,$

$$\rho I_a\frac{\partial}{\partial x_\beta}\left(\frac{q_\alpha q_\beta}{h}\right)=\rho\, I_a\left[\frac{\partial}{\partial x_2}\left(\frac{q_1 q_2}{h}\right)\right]\ . \tag{7.5}$$

Then term 3 is trivial:

$\alpha=1,$

$$-\rho g h\frac{\partial\zeta}{\partial x_\alpha}=\ -\rho g h\frac{\partial\zeta}{\partial x_1}\ . \tag{7.6}$$

Term 4 with β terms is expanded to give:

$\alpha = 1, \beta = 1,$

$$\rho\left(I_{p10}\frac{1}{2}h_s^2 + I_{p11}h_s\zeta\right)\frac{\partial}{\partial x_\alpha}\left(\frac{\partial^2 q_\beta}{\partial t \partial x_\beta}\right) = \rho\left(I_{p10}\frac{1}{2}h_s^2 + I_{p11}h_s\zeta\right)\frac{\partial}{\partial x_1}\left(\frac{\partial^2 q_1}{\partial t \partial x_1}\right) \tag{7.7}$$

$\alpha = 1, \beta = 2,$

$$\rho\left(I_{p10}\frac{1}{2}h_s^2 + I_{p11}h_s\zeta\right)\frac{\partial}{\partial x_\alpha}\left(\frac{\partial^2 q_\beta}{\partial t \partial x_\beta}\right) = \rho\left(I_{p10}\frac{1}{2}h_s^2 + I_{p11}h_s\zeta\right)\frac{\partial}{\partial x_1}\left(\frac{\partial^2 q_2}{\partial t \partial x_2}\right), \tag{7.8}$$

Term 5 contains both $\beta$and γ terms and is expanded to give the following four terms:

$\alpha = 1, \beta = 1, \gamma = 1,$

$$\rho\, I_{p2}\frac{1}{2}h_s^2\,\frac{\partial^2}{\partial x_\alpha \partial x_\beta}\left(\frac{q_\beta}{h}\frac{\partial q_\gamma}{\partial x_\gamma}\right) = \rho\, I_{p2}\frac{1}{2}h_s^2\,\frac{\partial^2}{\partial x_1^2}\left(\frac{q_1}{h}\frac{\partial q_1}{\partial x_1}\right), \tag{7.9}$$

$\alpha = 1, \beta = 1, \gamma = 2,$

$$\rho\, I_{p2}\frac{1}{2}h_s^2\,\frac{\partial^2}{\partial x_\alpha \partial x_\beta}\left(\frac{q_\beta}{h}\frac{\partial q_\gamma}{\partial x_\gamma}\right) = \rho\, I_{p2}\frac{1}{2}h_s^2\,\frac{\partial^2}{\partial x_1^2}\left(\frac{q_1}{h}\frac{\partial q_2}{\partial x_2}\right), \tag{7.10}$$

$\alpha = 1, \beta = 2, \gamma = 1,$

$$\rho\, I_{p2}\frac{1}{2}h_s^2\,\frac{\partial^2}{\partial x_\alpha \partial x_\beta}\left(\frac{q_\beta}{h}\frac{\partial q_\gamma}{\partial x_\gamma}\right) = \rho\, I_{p2}\frac{1}{2}h_s^2\,\frac{\partial^2}{\partial x_1 \partial x_2}\left(\frac{q_2}{h}\frac{\partial q_1}{\partial x_1}\right), \tag{7.11}$$

$\alpha = 1, \beta = 2, \gamma = 2,$

$$\rho\, I_{p2}\frac{1}{2}h_s^2\,\frac{\partial^2}{\partial x_\alpha \partial x_\beta}\left(\frac{q_\beta}{h}\frac{\partial q_\gamma}{\partial x_\gamma}\right) = \rho\, I_{p2}\frac{1}{2}h_s^2\,\frac{\partial^2}{\partial x_1 \partial x_2}\left(\frac{q_2}{h}\frac{\partial q_2}{\partial x_2}\right). \tag{7.12}$$

Term 6 is trivial:

$\alpha = 1,$

$$\sum_{w\alpha} - \sum_{b\alpha} = \sum_{w1} - \sum_{b1}\ . \tag{7.13}$$

Putting terms 1-6 together in 1HD, where all *y*-coordinate terms with subscript 2 cancel out gives:

$$\begin{aligned}\frac{\partial q}{\partial t} + I_a\left[\frac{\partial}{\partial x}\left(\frac{q^2}{h}\right)\right] = {} & -gh\frac{\partial \zeta}{\partial x} + \left(I_{p10}\frac{1}{2}h_s^2 + I_{p11}h_s\zeta\right)\left[\frac{\partial}{\partial x}\left(\frac{\partial^2 q}{\partial t\,\partial x}\right)\right] \\ & + \rho\, I_{p2}\frac{1}{2}h_s^2\left[\frac{\partial^2}{\partial x^2}\left(\frac{q}{h}\frac{\partial q}{\partial x}\right)\right] + \frac{\sum_{wx} - \sum_{bx}}{\rho}\end{aligned} \tag{7.14}$$

Appendix B

A numerical model to solve The Shallow Water Equations in 1HD in the *x*-coordinate has also been devised using a central difference scheme. Dropping all *y*-terms and ignoring wind shear and body forces, the mass and momentum equations become respectively:

$$\frac{\partial \zeta}{\partial t} + \frac{\partial q}{\partial x} = 0 \ , \tag{7.15}$$

Where: $q = Uh$, and

$$\frac{\partial q}{\partial t} + \frac{\partial (q^2/h)}{\partial x} = -gh\frac{\partial \zeta}{\partial x} - \frac{\tau_{bx}}{\rho} \ . \tag{7.16}$$

Rearranging, the temporal derivatives are given in terms of spatial derivatives:

$$\frac{\partial \zeta}{\partial t} = -\frac{\partial q}{\partial x} \ , \tag{7.17}$$

and

$$\frac{\partial q}{\partial t} = -\frac{\partial \left(\frac{q^2}{h}\right)}{\partial x} - gh\frac{\partial \zeta}{\partial x} - \frac{\tau_{bx}}{\rho} \ . \tag{7.18}$$

Applying the central difference scheme:

$$\frac{\partial \zeta}{\partial t}|_i^k = -\frac{q_{i+1}^k - q_{i-1}^k}{2\Delta x} \ , \tag{7.19}$$

and

$$\frac{\partial q}{\partial t}|_i^k = -\frac{\frac{q_{i+1}^2}{h_{i+1}} - \frac{q_{i-1}^2}{h_{i-1}}}{2\Delta x} - gh_i\frac{\zeta_{i+1} - \zeta_{i-1}}{2\Delta x} - \frac{\tau_{bxi}}{\rho} \ . \tag{7.20}$$

A second-order Adams-Bashforth time integration is then utilised, such that:

$$\zeta_i^{k+1} = \zeta_i^k + dt\left(1.5\frac{\partial \zeta}{\partial t}|_i^k - 0.5\frac{\partial \zeta}{\partial t}|_i^{k-1}\right) \ , \tag{7.21}$$

and

$$q_i^{k+1} = \zeta_i^k + dt\left(1.5\frac{\partial q}{\partial t}|_i^k - 0.5\frac{\partial q}{\partial t}|_i^{k-1}\right) \ . \tag{7.22}$$